Syndapin-2 Mediates Amyloid-β Transcytosis at the Brain Endothelium: Implications in Alzheimer's Disease

Diana M. Leite[1,2], Mohsen Seifi[3], Jerome D. Swinny[4] and Giuseppe Battaglia[1,2,5,6,*]

[1]*Department of Chemistry, University College London, London, United Kingdom;*
[2]*Institute for the Physics of Living Systems, University College London, London, United Kingdom;*
[3]*School of Sport, Health and Social Sciences, Solent University, Southampton, United Kingdom;*
[4]*School of Pharmacy and Biomedical Sciences, University of Portsmouth, Portsmouth, United Kingdom;*
[5]*Institute for Bioengineering of Catalonia (IBEC), The Barcelona Institute for Science and Technology (BIST), Barcelona, Spain;*
[6]*Catalan Institution for Research and Advanced Studies (ICREA), Barcelona, Spain.*
[*]*Corresponding author: Prof Giuseppe Battaglia, Christopher Ingold Building, Department of Chemistry, University College London, 20 Gordon Street, WC1H 0AJ, London, United Kingdom, Email:g.battaglia@ucl.ac.uk*

A faulty transport of amyloid-β (Aβ) across the blood-brain barrier (BBB), and its diminished clearance from the brain, contributes to neurodegenerative and vascular pathologies, including Alzheimer's disease (AD) and cerebral amyloid angiopathy, respectively. At the BBB, Aβ efflux transport is associated with the low-density lipoprotein receptor-related protein 1 (LRP1). However, the precise mechanisms governing the Aβ transport across the BBB, in health and disease, remain to be fully understood. New evidences suggest that LRP1 transcytosis occur through a tubular mechanism mediated by an F-BAR protein, syndapin-2. We show here that syndapin-2 is associated with Aβ clearance across the BBB. We further demonstrate whether risk factors for AD, Aβ expression and ageing, impact on native syndapin-2 expression in the brain endothelium, with syndapin-2 mediating Aβ transcytosis. Both increased Aβ expression and ageing significantly decreased expression of syndapin-2. These are mirrored by an alteration of the endosome-associated protein Rab5, with an increase of expression with Aβ accumulation and ageing. Collectively, our data reveal that the syndapin-2-mediated pathway and its balance with endosomal sorting at endothelial level are critical for the clearance of neuronally-derived Aβ, and thus proposing a new measure to assess AD and ageing, as well as, a potential target for counteracting the build-up of brain Aβ.

Introduction

Amyloid-β (Aβ), the end-product of the sequential processing of amyloid precursor protein (APP), is implicated in a host of normal [1] and pathological functions within the brain parenchyma [2] and blood vessels [3]. A crucial process in the APP-Aβ pathway is the effective removal of Aβ from the brain, via the endothelium, yet the precise mechanism and molecular machinery remains to be fully identified. The importance of identifying precisely how Aβ is transported from the brain is brought into sharp focus by the significant effect that impaired Aβ clearance has on brain and vascular health, over the course of lifetime. Indeed, increased Aβ expression in brain parenchyma is a hallmark of ageing and age-related neurodegenerative disorders, such as Alzheimer's disease (AD) [4–7]. Furthermore, the accumulation of Aβ in brain blood vessels contributes to cerebral amyloid angiopathy [8], which in turn is also a significant element of AD pathology spectrum [9]. Therefore, the intrinsic mechanisms involved in the clearance of Aβ, and how this changes with age, remains of a paramount importance in the understanding of healthy ageing and age-related disorders, such as AD.

The clearance of brain Aβ occurs mainly through the blood-brain barrier (BBB) ($\sim$ 85% of all brain Aβ) [10], and therefore neurovascular dysfunctions contribute to the defective clearance of Aβ in AD [11, 12]. Low-density lipoprotein receptor-related protein 1 (LRP1) is an essential efflux transporter for brain Aβ across the BBB [10, 13–17]. LRP1 is a multifunctional signalling and scavenger receptor consisting of a heavy chain that binds to a diversity of ligands, including apolipoprotein E (ApoE), α2-macroglobulin (α2M), and APP [18]. Importantly, a direct interaction of LRP1 and Aβ in blood vessels initiates clearance of Aβ from brain to blood *via* transcytosis [13]. Other receptors, such as glycoprotein 330 [19] and P-glycoprotein [20]), as well as Aβ-binding proteins, including ApoJ and ApoE [10, 21], appear to regulate transport exchanges of their complexes with Aβ across the BBB. Ageing is a prominent risk factor for the development of the sporadic form of AD. Mounting evidence indicates that LRP1 expression declines in brain blood vessels and parenchyma during normal ageing in rodents and humans, and is further reduced in AD individuals [10, 22–24]. Furthermore, validated genetic risk factors for AD, including ApoE E4 allele [25] and the gene encoding for phosphatidylinositol-binding clathrin assembly (PICALM) [26], are linked to diminished clearance Aβ *via* LRP1. At the brain endothelium, Aβ binding to the ectodomain of LRP1 enhances the binding of PICALM, which then initiates a PICALM/clathrin-dependent endocytosis of Aβ-LRP1 complexes through endocytic vesicles (Rab5 and Rab11) leading to Aβ transcytosis [26]. Consequently, a reduction of PICALM levels in AD impairs the mechanism of transcytosis of Aβ through LRP1/PICALM, and positively correlates with the Aβ pathology and deterioration of cognition [26]. In senile plaques, LRP1 ligands, including ApoE, α2M, urokinase-type plasminogem activator, tissue plasminogen activator and lactoferrin co-deposit with Aβ indicating a loss of LRP1 in AD [27]. Despite the amount of evidence demonstrating a fundamental role in the clearance of Aβ, how LRP1 controls transcytosis across the brain endothelium remains to be fully elucidated.

The importance of Aβ-LRP1 trafficking in AD pathogenesis is accentuated by the identification of several endocytic-related genes that augment the risk of late-onset AD, including PICALM, BIN1, RIN3 and CD2AP [28–30]. Hence, dysfunctions in endocytic pathways appear to contribute to the AD pathology. Recently, we have demonstrated that at the brain endothelium, LRP1 associates with elements of classical vesicular endocytosis pathway (including clathrin, dynamin-2, Rab5 and Rab7) as well as with syndapin-2 (or PACSIN-2) to facilitate a fast tubulation-driven transcytosis [31]. Syndapin-2 is a Fer-CIP4 homology-Bin/Amphiphysin/Rvs (F-BAR) protein and, due to this F-BAR domain, syndapin-2 senses and/or induces positive membrane curvature (i.e., membrane bends in the direction of the leaflet decorated by the protein forming invaginations) stabilising tubular carriers [32]. In addition, syndapin-2 contains a Src homology 3 (SH3) domain that binds to dynamin-2 and to the actin-nucleating protein N-WASP that, ultimately, regulates actin filaments [33, 34]. Our recent study demonstrated that syndapin-2 is abundantly expressed at the brain endothelium, and that syndapin-2 associates with LRP1 to drive tubular transcytosis [31]. This involvement of syndapin-2 in orchestrating LRP1-mediated tubular transcytosis, together with the recognised importance of LRP1 in Aβ clearance from the brain, raises the question whether syndapin-2 is involved in the transport of Aβ across the brain endothelium and contributes to the build-up of Aβ in the brain.

In the current study, we investigated the mechanism of LRP1 transcytosis mediated by syndapin-2, and reveal novel insights into the association of syndapin-2 with Aβ and its clearance at the brain endothelium, in health and amyloidosis. We demonstrate that syndapin-2 is expressed in the brain endothelium, in physical proximity with LRP1 and Aβ, and that syndapin-2 mediates Aβ transport across the BBB. In addition, we demonstrate that syndapin-2-mediated transcytosis is independent of early (EEA-1 and Rab5) and late (Rab7) vesicular endocytic proteins, but that the balance between the classical vesicular endocytosis and syndapin-2-mediated mechanisms at the brain endothelium is dependent on the expression level of syndapin-2. Finally, we reveal that syndapin-2 expression within the brain and endothelium is regulated by Aβ expression and ageing.

Collectively, our data demonstrate that syndapin-2 is a novel contributor for regulation of Aβ transport in in the brain in health and disease.

Results and Discussion

Syndapin-2 directly interacts with LRP1 at the brain endothelium. We first confirmed that syndapin-2 is endogenously expressed in brain endothelium, using brain endothelial cells (BECs). Immunoblotting of polarised BECs (bEnd3) confirmed robust expression of syndapin-2 (**Fig.S1A**), while immunofluorescence revealed that syndapin-2 immunoreactivity was localised to perinuclear vesicles and vesicular-tubular structures in BECs (**Fig.1A**). These syndapin-2 immunopositive tubular structures exhibited an estimated diameter of 500 nm and lengths up to ($\sim$ 2 μm) (**Fig.1B**), which is in accordance to the tubules found for syndapin-2 on mouse brain capillaries imaged by stimulated emission depletion (STED) microscopy [31]. The endogenous syndapin-2 subcellular distribution observed here in BECs was similar to that described in other cells, including human umbilical vein endothelial, COS7 and HeLa cells, in which the tubular structures were described at the membrane edges [35]. Having confirmed the expression and location of syndapin-2 in BECs, we then assessed whether it is associated with LRP1 and its ligand, the Aβ-binding protein ApoE, using a proximity ligation assay (PLA) (**Fig.1C,D**) (**Fig.S2**). In agreement with our previously published data [31], syndapin-2 was widely associated with LRP1, as evidenced by the abundance ($\sim$ 200 dots per cell) of PLA dots distributed throughout individual cells, with each PLA dot representing individual syndapin-2/LRP1 proteins located within 40 nm of another. Syndapin-2 expression was also located in a close proximity to ApoE ($\sim$ 250 dots per cell). Since ApoE is a cognate ligand of LRP1, and therefore expected to interact with this receptor, we validated the PLA by quantifying the association of LRP1 and ApoE (**Fig.1E**) (**Fig.S2**). Indeed, we observed a significant association between ApoE and LRP1 with a substantial number of dots ($\sim$ 80 dots per cell). Interestingly, the abundance of dots for ApoE/LRP1 was lower than that for syndapin-2/ApoE and syndapin-2/LRP1. This suggests that syndapin-2 may also associate with other receptors for ApoE and, most importantly, other ligands for LRP1. ApoE is of particular relevance to AD given its key role in facilitating Aβ transcytosis by LRP1 [36]. Syndapin-2 not only associates with the efflux transporter for Aβ (LRP1) but also with ApoE, which impacts the transport and clearance of Aβ across the brain endothelium (**Fig.1F**). This association of syndapin-2/LRP1 and LRP1/ApoE was also established in human brain microvascular endothelial cells (HBMEC) (**Fig.S3**). Based on these *in vitro* findings, we then confirmed the expression of syndapin-2 in native mammalian brain. Immunoblotting of whole mouse brain homogenates confirmed strong syndapin-2 expression in the brain (**Fig.S1B**). Immunofluorescence revealed that syndapin-2 expression is enriched in the hippocampus, particularly in CA3 and molecular layers of the dentate gyrus (**Fig.S1C**), as well as the molecular layer of the cerebellum (**Fig.S1D**), in close agreement with previously published reports [37]. The strong association of syndapin-2 with LRP1 in the native brain was confirmed by assessing the colocalisation of their respective immunoreactivity profiles within brain blood vessels, using fixed hippocampal tissue sections (**Fig.1G,H**). The strong association between syndapin-2 and LRP1 in brain endothelium was shown by the correlation coefficient value of 0.55$\pm$0.28 (n = 40 blood vessels) (**Fig.1G**). This correlation is clearly shown by the overlap of syndapin-2 and LRP1 labelling on lectin-labelled blood vessels (**Fig.1H**) with syndapin-2 and LRP1 outlining the blood vessels within the hippocampus. Hence, our data demonstrate that syndapin-2 is expressed in brain endothelium, and associates with proteins involved in the complex machinery of Aβ clearance through the BBB, namely, LRP1 and ApoE.

Syndapin-2 impacts on the balance between a tubular and vesicular transcytosis. Although transcytosis of LRP1 across the brain endothelium is well-established, the precise machinery involved in the intracellular trafficking of LRP1 is yet to be fully identified. In our recently published study [31], we demonstrated that LRP1-mediated transcytosis occurs either through classical endocytic vesicles or tubular structures stabilised by syndapin-2 [31]. To further understand the mechanism of transport mediated by syndapin-2, we investigated the association of syndapin-2 with other classical vesicular endocytic proteins, such as EEA-1, Rab5 and Rab7, in polarised BECs using a PLA. Rab5 GTPase and EEA-1 (a Rab5 effector protein) associate with early endosomal vesicles [38], while Rab7 is a GTPase that directs fusion of late endosomes with lysosomes leading to degradation of ligands [38]. PLA analyses indicated a negligible association of syndapin-2 with vesicular endocytic markers, as demonstrated by the low abundance of PLA dots (**Fig.2A-C**) (**Fig.S4**) in polarised BECs (< 10 dots per cell). This implies that syndapin-2 expression is largely not in the vicinity of either early or late endosomal vesicles. The stark contrast in the abundance of PLA dots obtained for syndapin-2/LRP1 ($\sim$ 200 dots) (**Fig.1C**) compared to that of syndapin-2 and EEA-1, Rab5 and Rab7 suggests that syndapin-2 association with LRP1 is independent of the classical vesicular trafficking of LRP1. In addition to the PLA, colocalisation analysis of syndapin-2 and EEA-1, Rab5 and Rab7 in polarised BECs also indicated no association between syndapin-2 and vesicular endocytic proteins with Pearson's correlation coefficients close to zero (**Fig.S5**). To assess whether this holds true within the mammalian brain, we investigated the

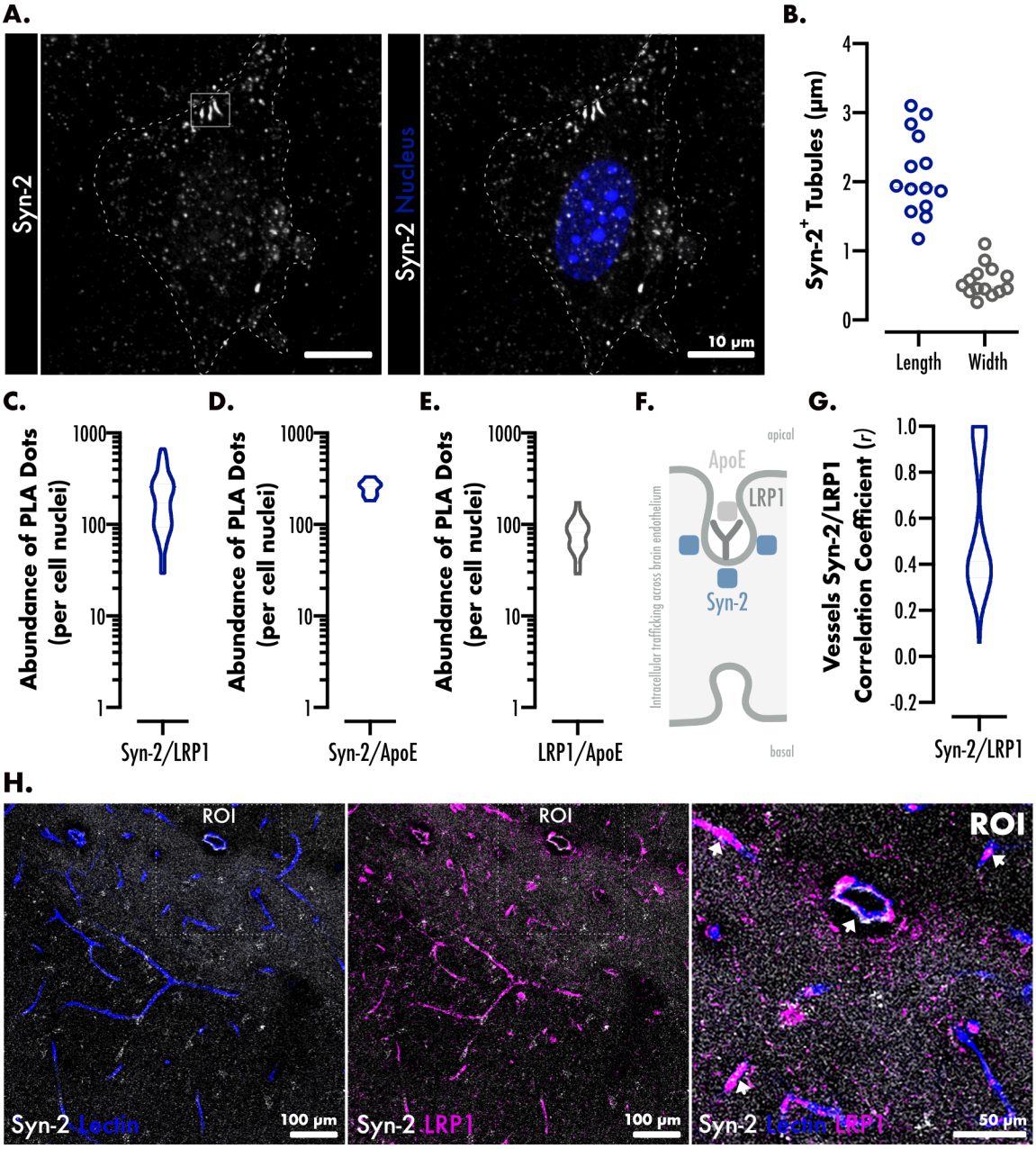

Figure 1: Syndapin-2 associates with LRP1 in the brain endothelium. (**A**) *In vitro* expression of syndapin-2 (in white) in polarised BECs, showing syndapin-2-tubular structures (highlighted in the boxed region). Nucleus is shown in blue. Dotted line represents the limits of the cell membrane. (**B**) Dimensions of syndapin-2-tubular structures within polarised BECs. Mean $\pm$ SD (n = 14). Abundance of PLA dots from proximity of (**C**) syndapin-2/LRP1, (**D**) syndapin-2/ApoE and (**E**) LRP1/ApoE in BECs. Violin plot of n = 10-20 images. (**F**) Schematic representation of the intracellular trafficking of LRP1/syndapin-2/ApoE complexes across BECs. (**G**) *Ex vivo* colocalisation of syndapin-2 and LRP1 in the blood vessels of WT mouse brains. Violin plot of n = 40 blood vessels. (**H**) Representative confocal images of the hippocampus (*stratum radiatum* of CA1 region) of mouse brain indicating the immunoreactivity for syndapin-2 (in white) within lectin-labelled brain blood vessels in blue (left panel) with that of LRP1 in magenta (middle panel). The panel on the right is a magnified view of a region of interest (ROI), illustrating the colocalisation (arrows) of syndapin-2 and LRP1 within the blood vessels.

colocalisation of syndapin-2 and Rab5 within blood vessels of WT mouse hippocampus (**Fig.2D**). Although we observed immunoreactivity for both syndapin-2 and Rab5 associated with the lectin-labelled brain blood vessels, 3D reconstructions of z-stacks acquired on blood vessels revealed little overlap of immunoreactivity for syndapin-2 and Rab5 (**Fig.2Di**). This further substantiates our data in BECs and is in agreement with previously a published study that demonstrated that syndapin-2 tubular structures in epithelial cells are not colocalised with EEA-1 and Rab5 [35].

Our PLA and colocalisation data suggest that LRP1 transcytosis mediated by syndapin-2 is not associated with the vesicular endocytic pathway. However, it is unclear whether these two pathways operate wholly independently, or they are capable of compensatory crosstalk to counteract any dysregulation that may arise in one another. To probe this further, we established BECs expressing low levels of syndapin-2, by knocking down the expression of syndapin-2 using short hairpin RNA (shRNA) [31]. Using a PLA, we evaluated whether this impacts on the level of association of LRP1 with syndapin-2 and vesicular endocytic proteins (EEA-1, Rab5 and Rab7) in BECs (**Fig.3**) (**Fig.S6**). It is important to highlight that the knockdown of syndapin-2 in BECs resulted in no significant effects on the BBB properties with monolayers showing dextran permeability values of 25.6 and 5.3 nm s^{-1} for 4 and 70 kDa dextrans, respectively [31]. We also confirmed that LRP1 expression remains unaltered with the knockdown of syndapin-2 (**Fig.S7**). The knockdown of syndapin-2 in BECs resulted in a reduction ($\sim$ 2-fold decrease in the number of PLA dots) of the abundance of LRP1/syndapin-2 dots compared to BECs transfected with a control shRNA (**Fig.3A**). In contrast, downregulation of syndapin-2 led to a significant increase in the association of LRP1 with early endosomal proteins EEA-1 and Rab5 ($\sim$ 2-fold increase in number of PLA dots) (**Fig.3B,C**), as well as the late endosomal protein Rab7 ($\sim$ 1.5-fold increase in number of PLA dots (**Fig.3D**). Thus, depletion of syndapin-2 levels triggers a substantial increase in the association of LRP1 with vesicular endocytic proteins, in particular EAA1 and Rab5, in a constant inverse proportion (i.e., a 2-fold reduction in LRP1/syndapin-2 led to 2-fold increase in LRP1/EEA-1 and RAB5). Collectively, under basal conditions, the syndapin-2-mediated LRP1 tubular trafficking appears to be independent of the vesicular trafficking. However, a decline in syndapin-2 expression levels pivots LRP1 trafficking towards the vesicular endocytic pathway as a compensatory mechanism in BECs (**Fig.3E**), thereby emphasising the importance of syndapin-2 expression levels in determining endothelial transport mechanisms.

Syndapin-2 interacts with Aβ and transports it across brain endothelium. Given the role of syndapin-2 in mediating LRP1 trafficking and the recognised importance of LRP1 in Aβ clearance across the brain endothelium [26], we next investigated whether syndapin-2 is also implicated in the transport of Aβ across BECs. Polarised BECs were incubated with FAM-Aβ (1-40) (500 nM) for 5 minutes [26], and the levels of FAM-Aβ-syndapin-2 colocalisation were assessed (**Fig.4A,B**). As depicted in **Fig.4A**, Aβ (1-40) was located within the cell cytoplasm in close proximity to immunoreactivity for syndapin-2. Horizontal orthogonal views (x, z) obtained from a z-stack of the *in vitro* monolayer of BECs revealed that colocalised syndapin-2-Aβ (1-40) profiles within the cell presented as elongated tubular-like structures (**Fig.4Ai**). Importantly, syndapin-2-Aβ complexes appeared not only at the apical and basal membranes but also within the cell, most likely *en route* from the basal to apical side. This suggests that syndapin-2 remains complexed with Aβ endocytic tubular structures during early and late stages of endocytosis and possibly acting together with cytoskeletal proteins such as, actin [34], to modulate membrane deformation into tubules [31]. To further investigate the association of syndapin-2 and FAM-Aβ, we quantified their degree of colocalisation within BECs (**Fig.4B**). The obtained correlation coefficient ($\sim$ 0.4) corroborated the strong interaction of syndapin-2 with Aβ. The close interaction of syndapin-2 with Aβ that stretch from the basal to apical membrane of BECs suggested that syndapin-2 is implicated in the transport of Aβ. To unequivocally assess the involvement of syndapin-2 in Aβ transcytosis, we next investigated whether depletion of syndapin-2 in BECs influences the transport of Aβ across our *in vitro* BBB model in the basal-to-apical direction (brain-to-blood). Using syndapin-2 knockdown BECs, we found that decrease in the expression of syndapin-2 in BECs resulted in a significant reduction in the basal-to-apical permeability of FAM-Aβ (1-40) (**Fig.4C**). The $\sim$ 50% reduction in the levels of syndapin-2 on BECs resulted in $\sim$ 20% decrease in basal-to-apical transcytosis of Aβ. Interestingly, we did not observe any significant changes in the apical-to-basal direction (blood-to-brain) FAM-Aβ (1-40) transcytosis (**Fig.S8**). Moreover, to assess the association of syndapin-2 and Aβ *ex vivo*, we investigated the colocalisation of syndapin-2 and Aβ immunoreactivity within coronal brain sections of the hippocampus of mouse brain (**Fig.4D**). Syndapin-2 was abundantly expressed in brain parenchyma and blood vessels, while Aβ was present at low levels (**Fig.4D**). 3D reconstructions obtained from two regions of interest (ROI) in **Fig.4D** clearly revealed the close association between syndapin-2 and Aβ within the lectin-labelled blood vessels (**Fig.4Di**). Collectively, these data provide the first demonstration for the implication of syndapin-2 in Aβ trafficking and transport across the brain endothelium.

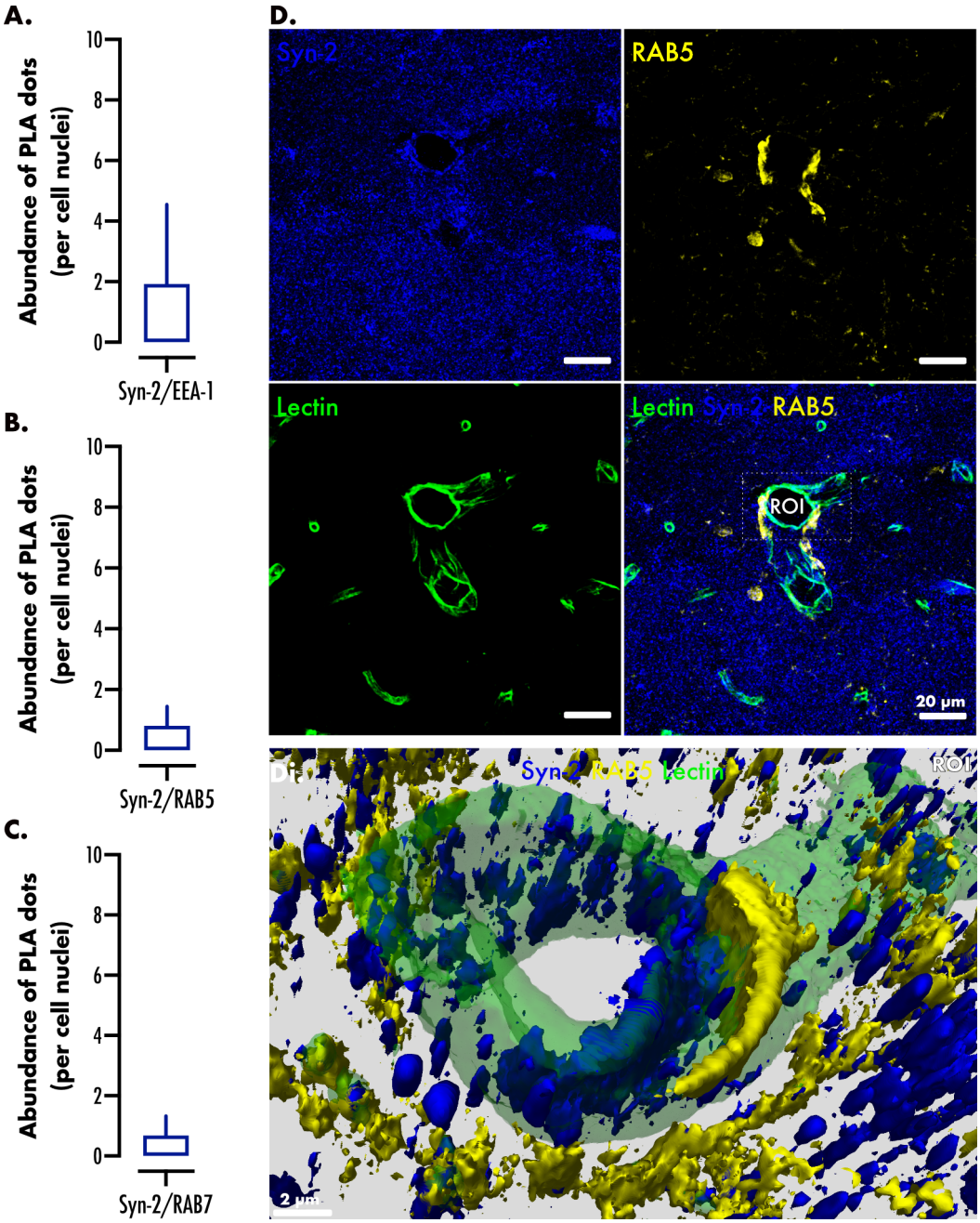

Figure 2: Syndapin-2 association with vesicular endocytic proteins in the brain endothelium. Quantification of the abundance of PLA dots representing the proximity of (**A**) syndapin-2/EEA-1, (**B**) syndapin-2/Rab5, and (**C**) syndapin-2/Rab7 in polarised BECs. Mean $\pm$ SD (n = 12 images). (**D**) *Ex vivo* expression of syndapin-2 (blue) and Rab5 (yellow) in lectin-labelled blood vessels (in green) in the hippocampus region of a WT mouse brain. (**D1**) A 3D reconstruction of a z-stack acquired on a region of interest (ROI) within a brain blood vessel, showing little overlap of immunoreactivity for syndapin-2 (blue) and Rab5 (yellow) in lectin-labelled blood vessels (in green).

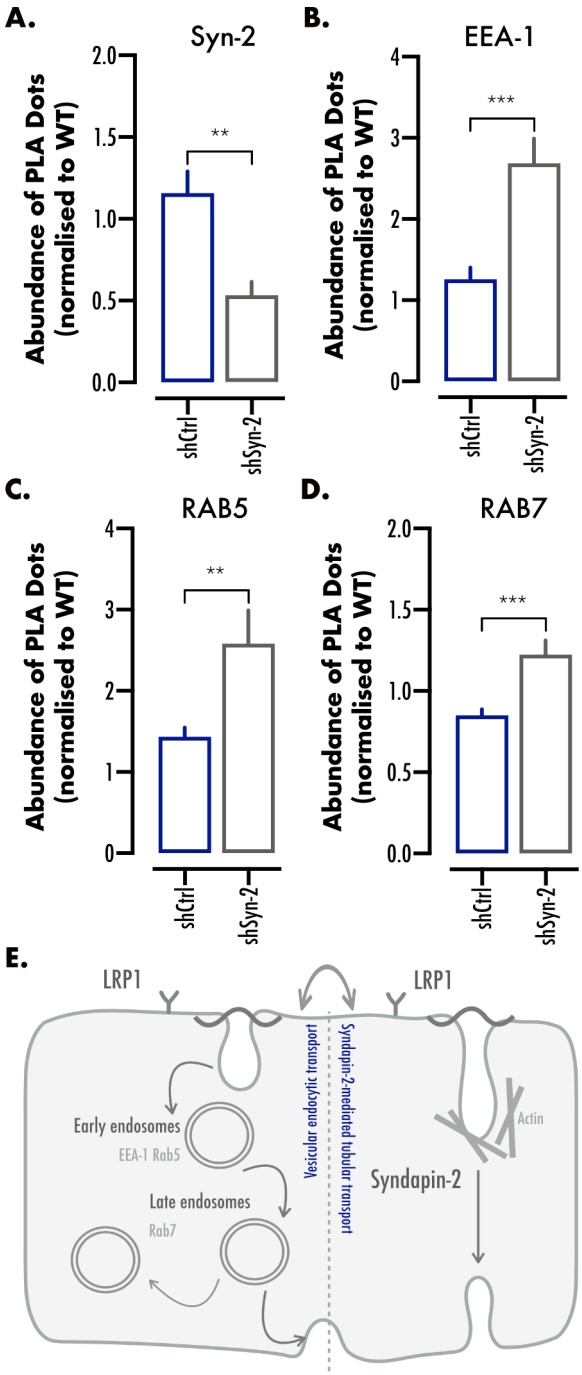

Figure 3: Balance between syndapin-2- and Rab-mediated intracellular trafficking of LRP1 in the brain endothelium. (**A**) Quantification of the abundance of PLA dots representing proximity of LRP1/syndapin-2 in control and syndapin-2 knockdown BECs. Quantification of the abundance of PLA dots showing proximity of LRP1 with (**B**) EEA-1, (**C**) Rab5 and (**D**) Rab7 in the control and syndapin-2 knockdown BECs. Abundance of dots was normalised to wild-type (WT) BECs. Mean $\pm$ SD (n = 20-30 images). ** P<0.01, *** P<0.001, comparing control (shCtrl) and syndapin-2 knockdown (shSyn-2) BECs. (**E**) Schematic representation showing the balance between the two mechanisms of intracellular trafficking for LRP1 in the brain endothelium.

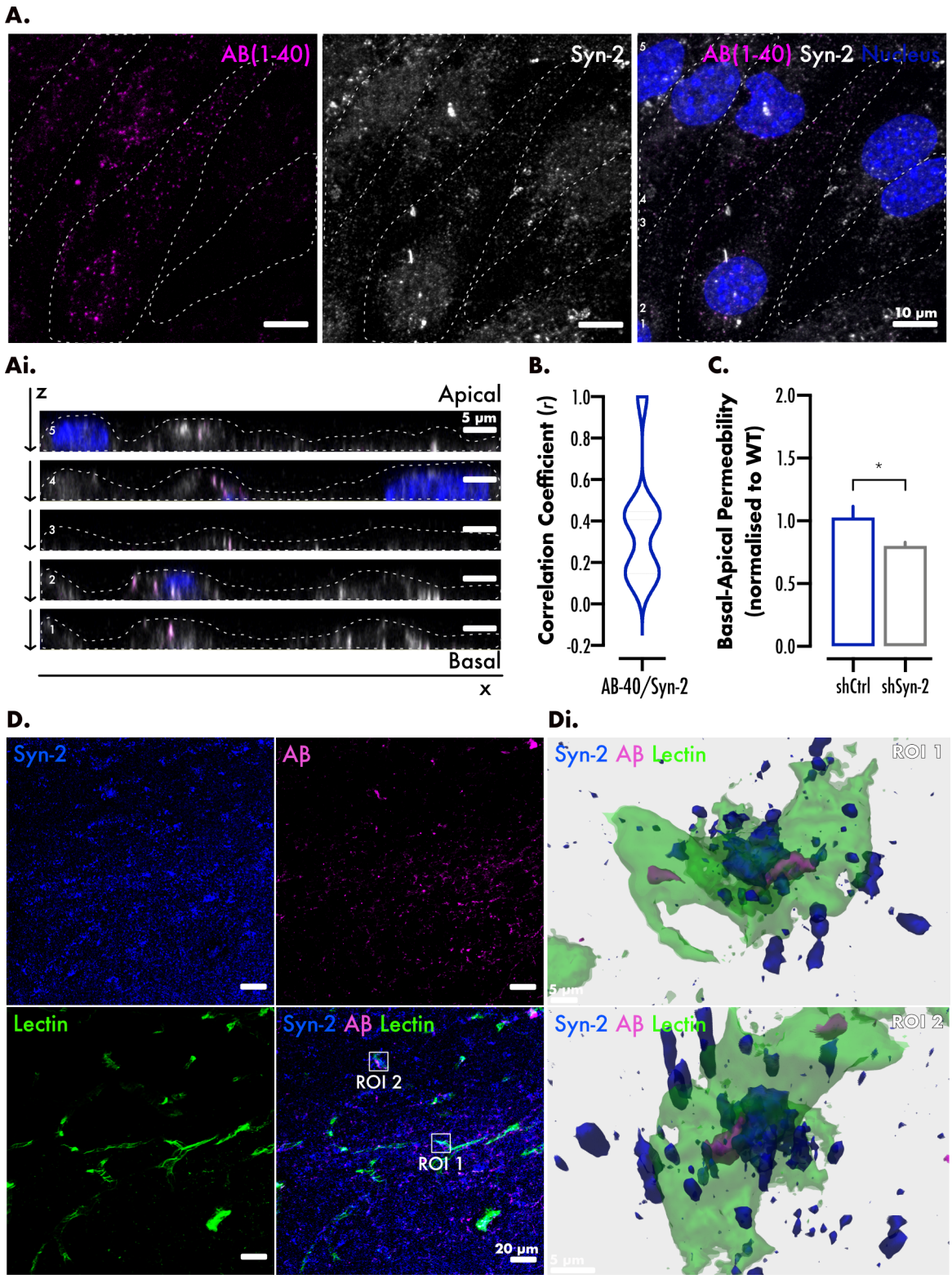

Figure 4: Syndapin-2 associates with amyloid-β in brain endothelium. (**A**) *In vitro* colocalisation of Aβ (1-40) and syndapin-2 (magenta) in polarised BECs treated with FAM-Aβ (1-40) (in white) for 5 minutes. Nuclei is shown in blue. (**Ai**) Z-projections of BECs showing the association of syndapin-2 and Aβ during transport of Aβ across the polarised BEC monolayer. (**B**) Quantification of the colocalisation of syndapin-2 and Aβ within BECs. Violin plot of n = 10 images. (**C**) *In vitro* permeability of FAM-Aβ (1-40) across polarised BECs expressing endogenous (shCtrl) and lower levels of syndapin-2 (shSyn-2) in the basal-to-apical (brain-to-blood) direction. Mean $\pm$ SD (n = 15). * P<0.05, comparing shCtrl and shSyn-2. Permeability values were normalised to wild-type (WT) BECs. (**D**) Representative confocal image of the hippocampal region of a WT mouse brain showing syndapin-2 (blue), Aβ (magenta) and lectin-labelled blood vessels (in green). (**Di**) 3D reconstruction of a z-stack acquired in two region of interest (ROI) depicting association of syndapin-2 and Aβ in the brain blood vessels.

Syndapin-2 expression is reduced in the APP-PS1 mouse model of AD. Since the downregulation of syndapin-2 expression within BECs resulted in reduced brain-to-blood Aβ transport (**Fig.4C**), we further probed the inter-dependence of this relationship by assessing the impact of increased native Aβ expression on syndapin-2 expression, using the APP-PS1 model. APP-PS1 mice accumulate Aβ at a young age and develop extracellular plaques consisting of fibrillary Aβ deposits, in the cerebral cortex and hippocampus, commencing at around 6 months of age [39], and confirmed in our mouse line, using 12-month old subjects (**Fig.5A**). Immunoreactivity for Aβ was distributed in the brain parenchyma and blood vessels, with signal for syndapin-2 localised to the wall of the vessels and surrounding intravascular Aβ deposits (**Fig.5Ai, ROI1**). Additionally, as observed in WT littermates (**Fig.4Di**), syndapin-2 immunoreactivity was located on the basal surface of blood vessels in close association with extravascular Aβ in APP-PS1 samples (**Fig.5Ai, ROI2**). This demonstrates that syndapin-2 is expressed in both WT and APP-PS1 brain, in association with Aβ, possibly facilitating its transport across the brain endothelium. To confirm that neuronally produced Aβ impacts on syndapin-2 expression in blood vessels, microvessels from WT and APP-PS1 mice were separated by a gradient centrifugation method performed on whole brains [26, 40], in which two fractions are obtained containing microvessels and parenchymal cells. Immunoblotting densiometry analysis confirmed that syndapin-2 expression in isolated microvessels from 12-months old APP-PS1 brains was significantly downregulated compared to WT (**Fig.5Bi**). Furthermore, in agreement with our *in vitro* data showing that syndapin-2 depletion triggers LRP1/Rab5 association (**Fig.3C**), *ex vivo* immunoblotting densiometry analysis revealed a significant increase ($\sim$ 3.5-fold) in the expression levels of Rab5 in the microvessels fraction of APP-PS1 brains compared to that of WT littermates (**Fig.5Bii**). The significant increase in the Rab5 levels in APP-PS1 samples, in parallel with the decrease in syndapin-2 expression, suggests that the balance between Rab5-mediated endocytosis or syndapin-2-mediated tubular transport, shifts dynamically depending on intrinsic syndapin-2 expression levels (**Fig.5Biii**). In the context of AD, Rab5 and Rab7 regulate Aβ endosomal trafficking in neurons [41]. However, at the brain endothelium, it has been shown that Rab5 and Rab11 are critical mediators for transcytosis of Aβ [26]. In the pathway mediated by PICALM, Aβ-LRP1 complexes colocalise with Rab5 and EEA-1-positive early endosomes but not with Rab7, a GTPase that directs fusion of late endosomes with lysosomes, or the lysosomal-specific proteins. Rather, Aβ-LRP1/PICALM colocalise with Rab11, a GTPase that regulates recycling of vesicles controlling transcytosis of ligands [42, 43], and inhibition or mutation of Rab11 inhibits the basal-to-apical transport of Aβ [26]. Furthermore, knockdown of PICALM inhibits Rab5 and Rab11 GTPase activity in endothelial monolayers treated with Aβ, indicating that PICALM binding to Rab5 and Rab11 is critical for maintaining these GTPases active during endosomal trafficking of Aβ. Based on this, the compensatory increased expression of Rab5 in APP-PS1 mice suggests that Aβ transport across the brain endothelium would still proceed through the vesicular pathway. However, PICALM expression levels are reduced in AD, which in turn results in diminished activation of Rab5 and Rab11 GTPases for endosomal trafficking of Aβ across BECs [26]. Thus, an enrichment of Rab5-positive endosomes might not necessarily result in a higher rate of transcytosis of Aβ as Rab5-mediated endocytosis is defective in AD. Interestingly, mounting evidence has pointed to the disturbance of Rab5-mediated endocytic pathways in early neuropathology in AD [44–46]. Studies of human donor tissue by Cataldo et al. [44, 45] have shown that at the earliest stages of AD, many neurons have increased levels of Aβ and exhibit abnormal overactivation of Rab5-positive early endosomes. These enlarged Rab5-positive endosomes exhibit immunoreactivity for other early endosomal markers (such as, EEA-1 and Rab4) and Aβ, implying that accumulation of Aβ in neurons is correlated with abnormal endosomes. Additionally, apart from PICALM, other studies have also identified alterations in the expression of Rab5-associated endocytic proteins, including BIN1 (amphiphysin-2) [29, 47] and RIN3 (Ras and Rab interactor 3 [30]), in AD [46]. It remains unclear how BIN1, RIN3 and other elements interact with the Rab5-mediated pathway in BECs. Nevertheless, it is plausible to speculate that alterations in these elements might also contribute to the enlargement of early endosomes that, ultimately, affect the trafficking of Aβ *via* Rab5-mediated endocytosis across BECs. Thus, apart from depletion of syndapin-2, other elements might also contribute to the overactivation of Rab5-positive endosomes observed in our AD mouse model.

Since syndapin-2 levels in isolated microvessels were comparable to those in the parenchyma, which contained neurons and glia, we also quantified the level of syndapin-2 and Rab5 in the parenchymal fraction of WT and APP-PS1 tissue (**Fig.5Ci,Cii**). Interestingly, syndapin-2 expression was also reduced in the APP-PS1 parenchyma by $\sim$50% compared to WT (**Fig.5Ci**), while Rab5 levels were increased (**Fig.5Cii**). This overexpression of Rab5 in the parenchyma of TG brains further confirms the previously reported overactivation of Rab5-positive endosomes in neurons of AD individuals [44, 45]. Similar to what occurs at the microvessels, syndapin-2 might be partly involved in the overactivation of early endosomes in the parenchyma. These findings also suggest a role for syndapin-2 in the trafficking of Aβ in neurons and glial cells, in which dysfunctional syndapin-2 levels are accompanied by an increased number of early endosomes (**Fig.5Cii**). These data suggest a role for syndapin-2 in neuronal Aβ trafficking that requires further investigations. Collectively, our data provide the first demonstration for the interaction of syndapin-2 with Aβ within the mammalian brain, and

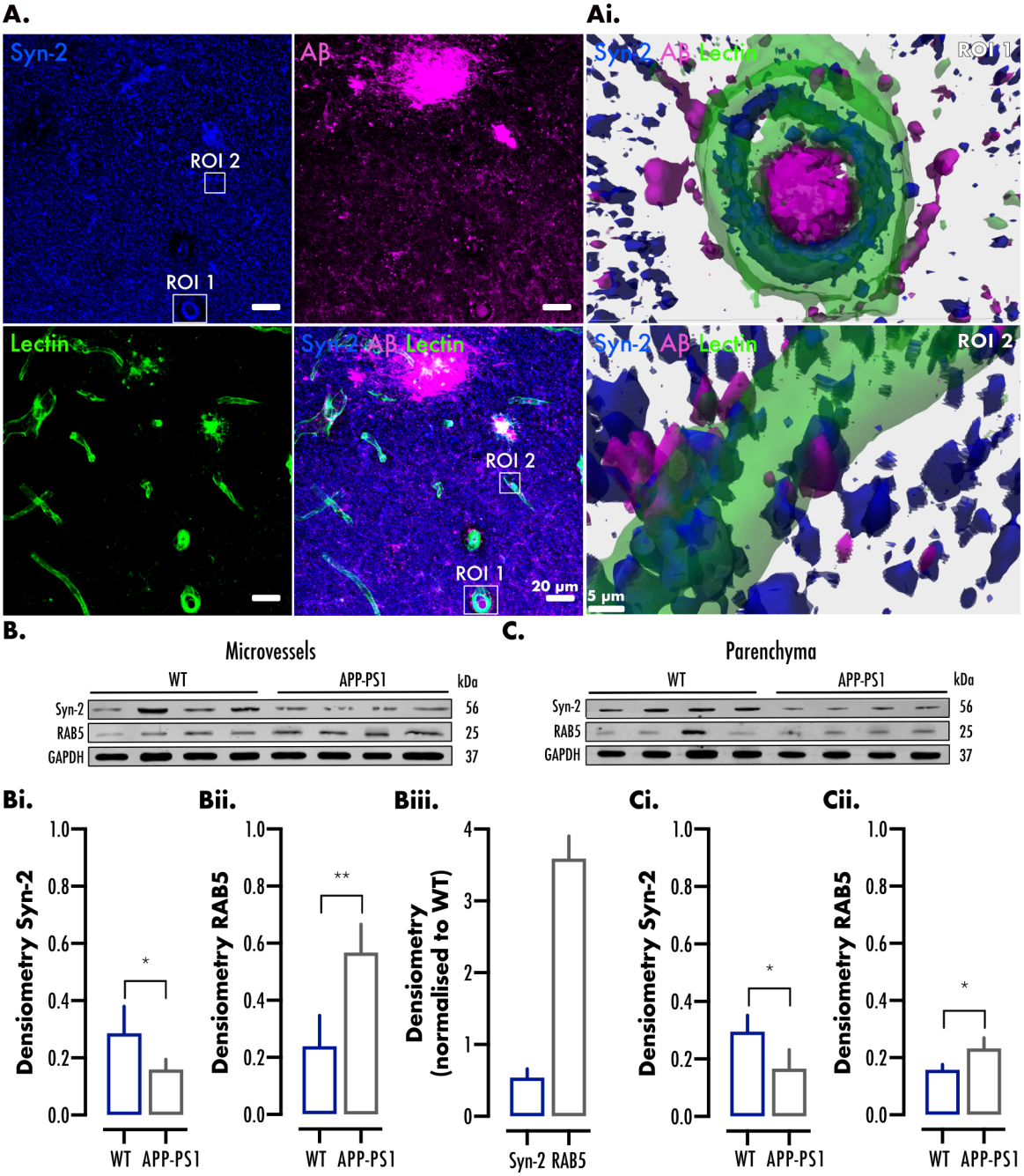

Figure 5: Brain amyloid-β production influences syndapin-2 expression in brain endothelium. (**A**) Representative confocal images of the hippocampus region of an AD mouse brain (APP-PS1) showing syndapin-2 (blue), Aβ (magenta) within the lectin-labelled blood vessels (in green). (**Ai**) 3D reconstructions of a z-stack acquired on two regions of interest (ROI1 and ROI2) within the hippocampus of an APP-PS1 brain exhibiting the association of syndapin-2 and Aβ within the blood vessels. (**B**) Immunoblotting for syndapin-2, Rab5 and GAPDH (loading control) in isolated microvessels from WT and APP-PS1 mice. Relative abundance of (**Bi**) syndapin-2 and (**Bii**) Rab5 in microvessels from WT and APP-PS1 brains determined by densiometry analysis relative to GAPDH. Mean $\pm$ SD (n = 4 animals). * P<0.05, ** P<0.01, comparing WT and APP-PS1. (**Biii**) Relative abundance of syndapin-2 and Rab5 in APP-PS1 brains in relation to the WT demonstrating an inverse correlation between syndapin-2 and Rab5 expression levels. (**C**) Immunoblotting for syndapin-2, Rab5 and GAPDH (loading control) in isolated parenchyma from WT and APP-PS1 mice. Relative abundance of (**Ci**) syndapin-2 and (**Cii**) Rab5 in parenchyma from WT and APP-PS1 brains determined by densiometry analysis relative to GAPDH. Mean $\pm$ SD (n = 4 animals). * P<0.05, comparing WT and APP-PS1.

its dysfunction in AD. Importantly, the levels of syndapin-2 and Rab5 in younger animals (4-months old) was also evaluated within the blood vessels, however no significant alterations were observed between WT and APP-PS1 brains (**Fig.S9**). Hence, this indicates that alterations in the expression level of syndapin-2 and Rab5 in blood vessels of AD brains are age-dependent.

Syndapin-2 expression decreases with age. Ageing is the most established risk factor for developing AD with sporadic AD accounting for $\sim$ 95% of all cases [48–50]. Within brain blood vessels, the expression of LRP1, an efflux transporter for Aβ across BECs, declines in normal ageing resulting in an accumulation of Aβ [23]. Furthermore, genes encoding proteins which interact with LRP1 and that are involved in Aβ transcytosis across the brain endothelium, including PICALM and ApoE, have been identified as some of the most prominent genetic risk factors for late-onset sporadic form of AD [51]. Given the interaction of syndapin-2 with LRP1 and ApoE, we next addressed whether syndapin-2 expression is altered by healthy ageing. We evaluated syndapin-2 and Rab5 expression in microvessels and parenchyma of 4- and 12-months old WT animals, respectively (**Fig.6A**) (**Fig.S9**). Immunoblotting densiometry analysis showed that the expression of syndapin-2 was significantly decreased (by $\sim$ 2-fold) in both microvessels and parenchyma of 12-months old brains compared to 4-months old (**Fig.6Ai**). GTPase Rab5 expression in the healthy animals shows no significant alterations, however a trend toward an increase in expression was noted in the microvessels (**Fig.6Aii**). Notably, we observed that the ratio of syndapin-2/Rab5 within brain microvessels, but not parenchyma, is diminished in 12-month-old compared to 4-months old brains (**Fig.6Aiii**). This suggests that in aged BECs, increased vesicular endocytic transport, partly mediated by Rab5 may compensate for diminished syndapin-2-mediated transcytosis. Therefore, the loss of syndapin-2 with ageing, especially at the microvessels, might be connected to the decline of LRP1 and faulty clearance of Aβ in healthy aged individuals. To determine whether the AD risk factors of age, and genetic mutations resulting in increased Aβ, are additive to their influence on syndapin-2 and Rab5 expression, we performed quantitative immunoblotting on brains obtained from 4- and 12-months old APP-PS1 brains (**Fig.6B**) (**Fig.S9**). In APP-PS1 brains, the expression of syndapin-2 was significantly reduced (by $\sim$ 6-fold) within the microvessels (**Fig.6Bi**), while Rab5 levels significantly increase in 12-months old compared to 4-months old APP-PS1 brains (**Fig.6Bii**). Consistent with these results, the syndapin-2/Rab5 expression ratio in AD was appreciably decreased in 12-months old brains (**Fig.6Biii**). Importantly, the decline in syndapin-2/Rab5 expression ratio within the microvessels in 12-months old APP-PS1 brains was much greater than that of WT animals (10-fold *versus* a 2-fold change in WT). Therefore, although the loss of syndapin-2 occurs naturally through the process of ageing, genetic predisposition to AD appears to accelerate this loss. Our results provide the first evidence for the involvement of syndapin-2 in Aβ clearance from the brain through LRP1-mediated transcytosis across the brain endothelium, and that the process of healthy ageing leads to a decline in the expression of syndapin-2, which is accelerated in AD.

Conclusions

In AD, Aβ pathology progresses in a temporospatial pattern through the connected brain structures, involving accumulation of neurotoxic Aβ in blood vessels and in the brain parenchyma [5, 12]. At the blood vessels, LRP1 acts as main efflux transporter for Aβ [10, 13, 14, 16]. Accordingly, a decline in the expression of LRP1 at BECs, which occurs with normal ageing and AD [22–24], leads to impaired clearance of Aβ across the brain endothelium. Mounting evidence suggest that, apart from the depletion of LRP1 at brain endothelium, dysfunctions in the vesicular endosomal trafficking also contribute to impaired transport of Aβ [26, 30, 44, 47]. Recently, we showed that aside from the classical vesicular endocytosis, LRP1 is also capable of tubular intracellular trafficking across BECs, a process which is mediated by syndapin-2 [31]. Syndapin-2 is a F-BAR domain-containing protein that senses and induces positive membrane curvature (i.e., invaginations), facilitating transcytosis of LRP1 *via* tubulation across the brain endothelium [31]. Hence, given the importance of LRP1 and its associated proteins in clearance of Aβ and pathophysiology of AD [26], we investigated whether syndapin-2 is also involved in Aβ clearance from the brain through BECs, and if syndapin-2-mediated transcytosis is altered in healthy ageing and AD.

Initially, we characterised the mechanism underlying syndapin-2-mediated LRP1 transcytosis across BECs. We demonstrated that syndapin-2 is present as tubular structures within BECs (*in vitro*) and blood vessels in the hippocampus of WT mouse brain (*ex vivo*), where syndapin-2 interacts with LRP1 (**Fig.1**). However, at a molecular level, we found that syndapin-2 is not associated with LRP1-related vesicular endocytic proteins, including EEA-1, Rab5 and Rab7 in polarised BECs, suggesting that syndapin-2-mediated tubular LRP1 transcytosis is distinct from the classical vesicular pathway (**Fig.2**). Furthermore, using BECs expressing low levels of syndapin-2, we revealed that downregulation of syndapin-2 triggers a considerable increase in the association of LRP1 with the classical vesicular endocytic proteins in BECs (**Fig.3**). These results suggest a

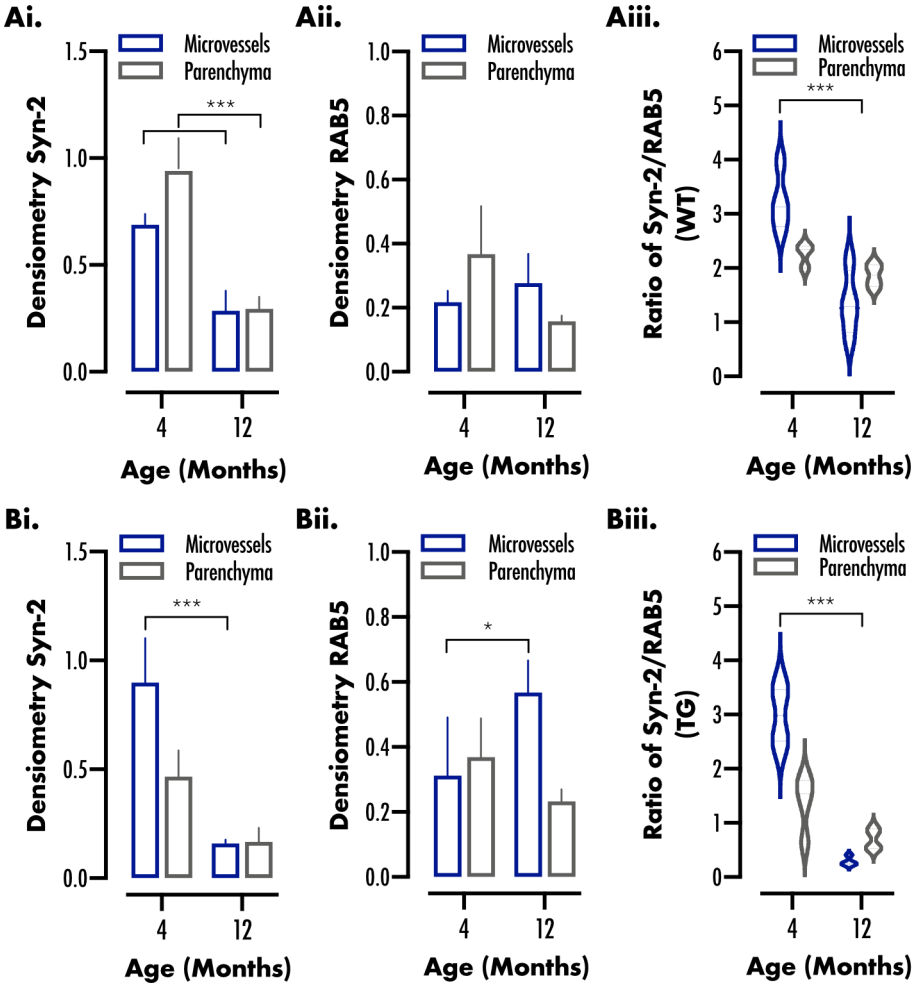

Figure 6: Imbalance in syndapin-2 expression is associated with ageing. (**A**) Expression level of syndapin-2 and Rab5 in microvessels and parenchyma isolated from 4- and 12-months old WT brains. Relative abundance of (**Ai**) syndapin-2 and (**Aii**) Rab5 in microvessels and parenchyma of 4- and 12-months old WT brains determined by densiometry analysis relative to GAPDH. Data are presented as mean $\pm$ SD (n = 4 animals). *** P<0.001, comparing 4- to 12-months old WT animals. (**Aiii**) Ratio of the expression of syndapin-2 and Rab5 in 4- to 12-months old animals. Violin plot of n = 4. ***P<0.001, comparing 4- to 12-months old animals. (**B**) Expression of syndapin-2 and Rab5 in microvessels and parenchyma isolated from 4- and 12-months old APP-PS1 brains. Relative abundance of (**Bi**) syndapin-2 and (**Bii**) Rab5 in microvessels and parenchyma isolated from 4- and 12-months old WT brains determined by densiometry analysis relative to GAPDH. Data are presented as mean $\pm$ SD (n = 4 animals). * P<0.05, *** P<0.001, comparing 4- to 12-months old APP-PS1 animals. (**Biii**) Ratio of the expression of syndapin-2 and Rab5 in 4- to 12-months old APP-PS1 brains. Violin plot of n = 4. ***P<0.001, comparing 4- to 12-months old animals.

balance between the two mechanisms with BECs compensating the lack of syndapin-2 with an increase of endosomal proteins to drive a vesicular endosomal trafficking of LRP1. To shed light on the involvement of syndapin-2 in Aβ clearance, we explored the interaction of syndapin-2 and Aβ at the brain endothelium. Here, we demonstrated that syndapin-2 is closely associated with Aβ in the brain endothelium *in vitro* and *ex vivo*, and it appears to be wraparound Aβ within the BECs (**Fig.4**). Importantly, we observed that downregulation of syndapin-2 on BECs impairs the basal-to-apical (brain-to-blood) transport of Aβ (**Fig.4**). In addition, the close association of syndapin-2 and Aβ within brain blood vessels was also present in brains from AD mice (**Fig.5**). However, we observed that syndapin-2 levels are significantly reduced in the microvessels and parenchyma of 12-months old AD brains compared to age-matched littermates, whereas Rab5 expression is increased (**Fig.5**). This elevated level of Rab5 may be a compensatory effect in response to a decline in the syndapin-2 levels, as we observed in our *in vitro* experiments in BECs (**Fig.5**). Nevertheless, this could also be due to previously shown dysfunctions in the vesicular endocytic endosomal trafficking in BECs in AD [26]. Finally, we showed that the expression of syndapin-2 is significantly diminished due to healthy ageing, which may contribute to accumulation of neurotoxic Aβ within aged brain (**Fig.6**). Importantly, the age-induced loss of syndapin-2 within the brain was much greater in our genetically modified AD mice, indicating that genetic predisposition to AD accelerates age-induced loss of syndapin-2 (**Fig.6**). Although syndapin-2 was altered in microvessels and parenchyma of healthy and AD mouse brains, these alterations were more pronounced in the microvessels implying a prominent role of syndapin-2 in the clearance of Aβ across the brain endothelium.

Collectively, our study provides the first demonstration of the involvement of syndapin-2 in LRP1-mediated Aβ clearance across BECs, and its potential role in the accumulation of neurotoxic Aβ within the brain in AD. Therefore, syndapin-2 appears as an important target for Aβ therapy.

Acknowledgements

G.B. thanks the ERC for the starting grant (MEViC 278793) and consolidator award (CheSSTaG 769798), the EPSRC/BTG Healthcare Partnership (EP/I001697/1), EPSRC Established Career Fellowship (EP/N026322/1), EPSRC/SomaNautix Healthcare Partnership EP/R024723/1, and Children with Cancer UK for the research project (16-227).

Competing Interests

The authors declare no competing financial interests.

Author Contributions

D.M.L designed, performed the experiments and analysed the data. M.S. performed experiments. J.D.S. supervised and supplied the animal work. G.B. supervised and managed the experimental work. All authors wrote the manuscript.

Materials and Methods

Materials. bEnd3 (CRL-2299) and Dulbecco's Modified Eagle's Medium (DMEM) were obtained from ATCC. Foetal bovine serum (FBS), penicillin/streptomycin, phosphate-buffered saline (PBS, pH 7.4), 0.25% trypsin-EDTA solution and rat tail collagen I were obtained from Sigma-Aldrich. Polybrene, syndapin-2 shRNA and control shRNA lentiviral particles were obtained from Santa Cruz Biotechnology. Transwell permeable support polyester membranes (0.4 μm, 1.12 cm^{-2}) were obtained from Corning Inc. Paraformaldehyde (PFA), Triton X-100, normal horse serum, FITC-conjugated lectin, PLA probes (anti-rabbit PLUS and anti-mouse MINUS), Duolink detection reagent orange, radioimmunoprecipitation (RIPA) buffer, Tween-20, dextran (60-76 kDa) and bovine serum albumin (BSA) were also obtained from Sigma-Aldrich. Protease inhibitors, BCA protein assay kit, and Laemmli sample buffer (x4) were purchased from Biorad. 5-Fluorescein-amyloid-β protein (1-40) was obtained from Bachem. 4',6-diamidino-2-phenylindole (DAPI) and Leica standard immersion oil were purchased from Thermo Fisher Scientific. Vectashield Mounting Media was obtained from Vector Labs. All antibodies used are listed in Table 1 in Supporting Information.

Animals. All procedures involving animal experiments were approved by the Animal Welfare and Ethical Review Body of the University of Portsmouth and were performed by a personal license holder under a Home Office-issued project licence, in accordance with the Animals (Scientific Procedures) Act 1986 (UK). Male C57BL/6J mice were used to investigate the native association of syndapin-2 with Aβ. APP-PS1 transgenic mouse model of AD [39], which carries mutations for APP and presenilin-1 (APPswe and PSEN1dE9, respectively) resulting in increased Aβ production, was used to investigate the effect of Aβ on syndapin-2 expression levels. This line was maintained by crossing transgenic APP-PS1 with C57BL/6J wild-type (WT) mice. In all experiments, the WT littermates were used as controls for APP-PS1 animals. For the ageing studies, 4- and 12-months old WT and APP-PS1 animals were used to investigate the effect of ageing in the expression levels of syndapin-2. All animals were bred in-house in a temperature- and humidity-controlled environment under a 12-hour light/dark cycle with free access to standard chow and water.

Cell Culture. Mouse brain endothelial cells bEnd3 were used between passage 20-30. bEnd3 were grown in DMEM supplemented with 10% (v/v) FBS, and 100 IUL mL^{-1} penicillin/100 mg mL^{-1} streptomycin. Short hairpin RNA (shRNA) lentiviral particles were used to generate a stable cell line expressing lower levels of syndapin-2 [31]. Briefly, bEnd3 cells were seeded onto a 6-well plate at a density of 100,000 cells per well and grown overnight. At 50% of confluence, cells were treated with the shRNA lentiviral particles in DMEM supplemented with polybrene (5 μg mL^{-1}), and further incubated overnight. On the next day, media was replaced and cells were maintained for 2 days. Stable clones expressing shRNA were selected by puromycin (5 μg mL^{-1}). Syndapin-2 knockdown was confirmed by Western blot and immunofluorescence. bEnd3 transfected with control shRNA lentiviral particles were used as a negative control. Both syndapin-2 knockdown and shRNA control bEnd3 were cultured in DMEM supplemented with FBS, penicillin/streptomycin, and puromycin. Cells were maintained at 37 °C in an atmosphere of 5% CO_2. For subculture, cells were washed with PBS twice, incubated with 0.25% trypsin-EDTA for 3 minutes, centrifuged and resuspended in fresh media. Media was changed every 2-3 days.

***In Vitro* BBB Model.** To obtain a polarised monolayer, bEnd3 cells were seeded at 25,000 cells per cm^{-2} in collagen I-coated polyester transwells. Cells were grown for 3 days to reach confluency, and then the media in the basal side of the Transwell was replaced to serum-free DMEM. On day 6, transendothelial resistance and permeability of dextrans (4 and 70 kDa) was assessed, as previously reported [31].

Proximity Ligation Assay. Polarised bEnd3 were washed twice with PBS, fixed in 4% (w/v) PFA in PBS for 15 minutes and permeabilised with 0.1% (w/v) Triton X-100 in PBS for 10 minutes. Proximity ligation assay (PLA) was carried out by using Duolink probes and detection reagents according to the supplier's instructions. Briefly, monolayers were incubated with Duolink blocking solution for 1 hour at 37 °C and then incubated with the two antibodies targeting each protein of interest overnight at 4 °C. Subsequently, cells were incubated with Duolink PLA probes (anti-rabbit and anti-mouse) for 1 hour at 37 °C, washed and incubated with Duolink ligase and polymerase enzymes for 30 and 100 minutes, respectively. As a negative control, PLA protocol was followed with the exception of the addition of the primary antibodies to determine the specificity of the PLA probes. Nuclei were counterstained by incubation with DAPI for 10 minutes. Membranes were mounted in glass coverslips using Vectashield Mounting Media. Images were acquired using a Leica TCS SP8 confocal microscope, via sequential scan to reduce fluorophore bleed-through, with a 63x oil immersion objective. Z-stacks (10-20 stacks per sample) were collected (20 optical sections) and fluorescence intensity of the PLA signal was quantified using ImageJ. Abundance of PLA signal was normalised by the number of nuclei in each z-stack image. List of antibodies in Supporting Information.

Immunofluorescence. Polarised bEnd3 were washed twice with PBS, fixed in 4% (w/v) PFA in PBS for 15 minutes, permeabilised with 0.1% (w/v) Triton X-100 in PBS for 10 minutes and incubated with 5% (w/v) BSA in PBS for 1 hour at room temperature. Subsequently, bEnd3 cells were incubated with primary antibodies diluted in 1% (w/v) BSA and 0.01% (w/v) Triton X-100 in PBS overnight at 4 °C, washed with PBS and incubated with the corresponding secondary antibody at room temperature for 2 hours. Nuclei were counterstained by incubation with DAPI for 10 minutes. Transwell membranes were excised and mounted on glass coverslips with Vectashield Mounting Media. Images were acquired using a Leica TCS SP8 confocal microscope using a 63x oil immersion objective (z-stacks of 20 optical sections). Images were processed on ImageJ. List of antibodies in Supporting Information.

Adult WT and TG mice were anesthetised with isoflurane and pentobarbitone (1.25 mg Kg^{-1} of body weight, intraperitoneal) and transcardially perfused using fixative containing 1% (w/v) PFA and 15% (v/v) saturated picric acid in 0.1 M phosphate buffer (PB, pH 7.4), according to previously reported protocols [52]. After perfusion, brains were dissected from the skull, post-fixed overnight at room temperature in fixative solution, sectioned with a vibratome and stored in a solution containing 0.1 M PB and 0.05% (v/v) sodium azide until further use. Coronal sections of the hippocampal region of WT and TG mice brains were incubated in 20% (v/v) normal horse serum containing 0.3% (w/v) Triton X-100 in PBS for 2 hours at room temperature under gentle agitation. Then, the tissue sections were incubated with the primary antibodies diluted in 0.3% (w/v) Triton X-100 in PBS overnight at 4 °C. Following primary antibodies, sections were washed with PBS and incubated with the appropriate secondary antibodies and FITC-conjugated lectin (1:200) for 2 hours at room temperature under agitation. Tissue sections were washed with PBS and mounted on glass coverslips with Vectashield Mounting Media. Images were acquired with a Leica TCS SP8 confocal microscope using a 20x objective in a sequential mode to reduce fluorophore bleed-through. Z-stacks were acquired (20 optical sections) with images being processed on ImageJ or Leica LAS-X software for rendering 3D reconstructions.

***In Vitro* Permeability of Aβ (1-40).** To evaluate the permeability of Aβ across the polarised bEnd3 monolayers, FAM-Aβ(1-40) (500 nM) was added to the basal side of the transwell to measure basal-to-apical permeability. Samples were collected from the apical side, and fresh medium was added to replace the volume. FAM-Aβ(1-40) fluorescence was measured in a 96-well plate using a Spark Multimode microplate reader (Tecan). Apparent permeability was calculated as:

$$P = \frac{V_r}{C_0 A} \frac{dQ}{dt} \tag{1}$$

with V_r being the volume of the receptor (apical), C_0 the initial Aβ concentration, A the total surface area of the transwell membrane, and $\frac{dQ}{dt}$ the transport rate calculated as the gradient of mass over time.

Western Blot. Microvessels and capillary-depleted fractions were prepared from WT and TG mice brains, as previously described [26]. WT and TG mice were anesthetised, decapitated and the brains were carefully collected from the skull. Brains were homogenised in a 4-fold excess volume of ice-cold buffer solution: 10 mM HEPES, 141 mM NaCl, 4 mM KCl, 2.8 mM $CaCl_2$, 1 mM $MgSO_4$, 1 mM NaH_2PO_4 and 10 mM glucose, pH 7.4, in a glass homogeniser (10-15 strokes). Homogenate was suspended in an equal volume of 26% (w/v) dextran (64-76 kDa), mixed, and centrifuged at 15,800 g for 10 minutes at 4 °C. Pellet containing the brain microvessels was carefully separated from the supernatant containing capillary-depleted brain (parenchyma). Both fractions, microvessels and parenchyma, were washed twice in ice-cold buffered solution by centrifugation at 15,800 g for 10 minutes. Brain microvessels and parenchyma fractions were resuspended in RIPA lysis buffer containing protease inhibitors, centrifuged for 20 minutes, and the supernatant used for Western blot analysis. Protein levels in the lysates were determined using a BCA Protein Assay Kit (Bradford). Lysates were mixed with Laemmli sample buffer, and proteins (25 μg) were separated on 10% SDS polyacrylamide gels and transferred to polyvinylidene difluoride (PVDF) membranes. All membranes were blocked with 5% (w/v) non-fat milk in Tris-buffered saline (TBS) containing 0.1% (w/v) Tween-20 (TBS-T) for 1 hour and then incubated at 4 °C with the primary antibody overnight. After washing with TBS-T three times, membranes were incubated with the corresponding secondary antibody for 1 hour at room temperature, washed with TBS-T and imaged using an Odyssey CLx (LI-COR Biosciences). All membranes were also probed for GAPDH as a loading control.

Statistical Analysis. Statistical analyses and graphical evaluations were performed with Prism 8.0 (GraphPad Inc.). All data are represented as the mean and standard deviation (SD) unless stated otherwise. Statistical comparisons were carried out using Student's t-test, One-Way or Two-Way ANOVA followed by a post-hoc test. A $p < 0.05$ was considered statistically significant.

References

[1] G.-F. Chen, T.-H. Xu, Y. Yan, Y.-R. Zhou, Y. Jiang, K. Melcher, and H. E. Xu. Amyloid beta: structure, biology and structure-based therapeutic development. *Acta Pharmacologica Sinica*, 38(9):1205–1235, 2017.

[2] H. M. Brothers, M. L. Gosztyla, and S. R. Robinson. The physiological roles of amyloid-βpeptide hint at new ways to treat alzheimer's disease. *Frontiers in Aging Neuroscience*, 10:118–118, 2018.

[3] E. E. Smith and S. M. Greenberg. Beta-amyloid, blood vessels, and brain function. *Stroke*, 40(7):2601–2606, 2009.

[4] J. Hardy and D. J. Selkoe. The amyloid hypothesis of alzheimer's disease: Progress and problems on the road to therapeutics. *Science*, 297(5580):353–356, 2002.

[5] B. V. Zlokovic, R. Deane, J. Sallstrom, N. Chow, and J. M. Miano. Neurovascular pathways and alzheimer amyloid β-peptide. *Brain Pathology*, 15(1):78–83, 2005.

[6] K. Blennow, M. J. de Leon, and H. Zetterberg. Alzheimer's disease. *The Lancet*, 368(9533):387–403, 2006.

[7] D. J Selkoe and J. Hardy. The amyloid hypothesis of alzheimer's disease at 25 years. *EMBO Molecular Medicine*, 8(6):595–608, 2016.

[8] A. Charidimou, G. Boulouis, M. E. Gurol, C. Ayata, B. J. Bacskai, M. P. Frosch, A. Viswanathan, and S. M. Greenberg. Emerging concepts in sporadic cerebral amyloid angiopathy. *Brain*, 140(7):1829–1850, 2017.

[9] A. Serrano-Pozo, M. P. Frosch, E. Masliah, and B. T. Hyman. Neuropathological alterations in alzheimer disease. *Cold Spring Harbor Perspectives in Medicine*, 1(1):a006189, 2011.

[10] M. Shibata, S. Yamada, S. R. Kumar, M. Calero, J. Bading, B. Frangione, D. M. Holtzman, C. A. Miller, D. K. Strickland, J. Ghiso, and B. V. Zlokovic. Clearance of alzheimer's amyloid-ss(1-40) peptide from brain by ldl receptor-related protein-1 at the blood-brain barrier. *The Journal of Clinical Investigation*, 106(12):1489–1499, 2000.

[11] C. Iadecola. Neurovascular regulation in the normal brain and in alzheimer's disease. *Nature Reviews Neuroscience*, 5(5):347–360, 2004.

[12] B. V Zlokovic. The blood-brain barrier in health and chronic neurodegenerative disorders. *Neuron*, 57(2):178–201, 2008.

[13] R. Deane, Z. Wu, A. Sagare, J. Davis, S. Du Yan, K. Hamm, F. Xu, M Parisi, B LaRue, H W Hu, P. Spijkers, H. Guo, X. Song, P. J. Lenting, W. E. Van Nostrand, and B. V. Zlokovic. Lrp/amyloid beta-peptide interaction mediates differential brain efflux of abeta isoforms. *Neuron*, 43(3):333–344, 2004.

[14] R. D. Bell, A. P. Sagare, A. E. Friedman, G. S. Bedi, D. M. Holtzman, R. Deane, and B. V. Zlokovic. Transport pathways for clearance of human alzheimer's amyloid beta-peptide and apolipoproteins e and j in the mouse central nervous system. *Journal of Cerebral Blood Flow and Metabolism*, 27(5):909–918, 2007.

[15] T. Kanekiyo, C.-C. Liu, M. Shinohara, J. Li, and G. Bu. Lrp1 in brain vascular smooth muscle cells mediates local clearance of alzheimer's amyloid-β. *Journal of Neuroscience*, 32(46):16458–16465, 2012.

[16] S. E. Storck, S. Meister, J. Nahrath, J. N. Meißner, N. Schubert, A. Di Spiezio, S. Baches, R. E. Vandenbroucke, Y. Bouter, I. Prikulis, C. Korth, S. Weggen, A. Heimann, M. Schwaninger, T. A. Bayer, and C. U. Pietrzik. Endothelial lrp1 transports amyloid-β1–42 across the blood-brain barrier. *The Journal of Clinical Investigation*, 126(1):123–136, 2016.

[17] B. Van Gool, S. E. Storck, S. M. Reekmans, B. Lechat, P. L. S. M. Gordts, L. Pradier, C. U. Pietrzik, and A. J. M. Roebroek. Lrp1 has a predominant role in production over clearance of aβin a mouse model of alzheimer's disease. *Molecular Neurobiology*, 56(10):7234–7245, 2019.

[18] J. Herz and D. K. Strickland. Lrp: a multifunctional scavenger and signaling receptor. *The Journal of Clinical Investigation*, 108(6):779–784, 2001.

[19] B. V. Zlokovic, C. L. Martel, E. Matsubara, J. G. McComb, G. Zheng, R. T. McCluskey, B. Frangione, and J. Ghiso. Glycoprotein 330/megalin: probable role in receptor-mediated transport of apolipoprotein j alone and in a complex with alzheimer disease amyloid beta at the blood-brain and blood-cerebrospinal fluid barriers. *Proceedings of the National Academy of Sciences*, 93(9):4229–4234, 1996.

[20] J. R. Cirrito, R. Deane, A. M. Fagan, M. L. Spinner, M. Parsadanian, M. B. Finn, H. Jiang, J. L. Prior, A. Sagare, K. R. Bales, S. M. Paul, B. V. Zlokovic, D. Piwnica-Worms, and D. M. Holtzman. P-glycoprotein deficiency at the blood-brain barrier increases amyloid-beta deposition in an alzheimer disease mouse model. *The Journal of Clinical Investigation*, 115(11):3285–3290, 2005.

[21] B. V. Zlokovic. Cerebrovascular transport of alzheimer's amyloid beta and apolipoproteins j and e: possible anti-amyloidogenic role of the blood-brain barrier. *Life Sciences*, 59(18):1483–1497, 1996.

[22] J. E. Donahue, S. L. Flaherty, C. E. Johanson, J. A. Duncan, G. D. Silverberg, M. C. Miller, R. Tavares, W. Yang, Q. Wu, E. Sabo, V. Hovanesian, and E. G. Stopa. Rage, lrp-1, and amyloid-beta protein in alzheimer's disease. *Acta Neuropathologica*, 112(4):405–415, 2006.

[23] G. D. Silverberg, A. A. Messier, M. C. Miller, J. T. Machan, S. S. Majmudar, E. G. Stopa, J. E. Donahue, and C. E. Johanson. Amyloid efflux transporter expression at the blood-brain barrier declines in normal aging. *Journal of Neuropathology and Experimental Neurology*, 69(10):1034–1043, 2010.

[24] D. Osgood, M. C Miller, A. A Messier, L. Gonzalez, and G. D Silverberg. Aging alters mrna expression of amyloid transporter genes at the blood-brain barrier. *Neurobiology of Aging*, 57:178–185, 2017.

[25] R. Deane, A. Sagare, K. Hamm, M. Parisi, S. Lane, M. B. Finn, D. M. Holtzman, and B. V. Zlokovic. Apoe isoform-specific disruption of amyloid β peptide clearance from mouse brain. *The Journal of Clinical Investigation*, 118(12):4002–4013, 2008.

[26] Z. Zhao, A. P. Sagare, Q. Ma, M. R. Halliday, P. Kong, K. Kisler, E. A. Winkler, A. Ramanathan, T. Kanekiyo, G. Bu, N. C. Owens, S. V. Rege, G. Si, A. Ahuja, D. Zhu, C. A. Miller, J. A. Schneider, M. Maeda, T. Maeda, T. Sugawara, J. K. Ichida, and B. V. Zlokovic. Central role for picalm in amyloid-βblood-brain barrier transcytosis and clearance. *Nature Neuroscience*, 18(7):978–987, 2015.

[27] G. W. Rebeck, S. D. Harr, B. T. Hyman, and D. K. Strickland. Multiple, diverse senile plaque–associated proteins are ligands of an apolipoprotein e receptor, the α2-macroglobulin receptor/low-density-lipoprotein receptor—related protein. *Annals of Neurology*, 37(2):211–217, 1995.

[28] D. Harold, R. Abraham, P. Hollingworth, R. Sims, A. Gerrish, M. L. Hamshere, J. S. Pahwa, V. Moskvina, K. Dowzell, A. Williams, N. Jones, C. Thomas, A. Stretton, A. R. Morgan, S. Lovestone, J. Powell, P. Proitsi, M. K. Lupton, C. Brayne, D. C Rubinsztein, M. Gill, B. Lawlor, A. Lynch, K. Morgan, K. S. Brown, P. A. Passmore, D. Craig, B. McGuinness, S. Todd, C. Holmes, D. Mann, A. D. Smith, S. Love, P. G. Kehoe, J. Hardy, S. Mead, N. Fox, M. Rossor, J. Collinge, W. Maier, F. Jessen, B. Schürmann, R. Heun, H. van den Bussche, I. Heuser, J. Kornhuber, J. Wiltfang, M. Dichgans, L. Frölich, H. Hampel, M. Hüll, D. Rujescu, A. M. Goate, J. S. K. Kauwe, C. Cruchaga, P. Nowotny, J. C. Morris, K. Mayo, K. Sleegers, K. Bettens, S. Engelborghs, P. P. De Deyn, C. Van Broeckhoven, G. Livingston, N. J Bass, H. Gurling, A. McQuillin, R. Gwilliam, P. Deloukas, A. Al-Chalabi, C. E. Shaw, M. Tsolaki, A. B. Singleton, R. Guerreiro, T. W. Mühleisen, M. M. Nöthen, S. Moebus, K.-H. Jöckel, N. Klopp, H.-E. Wichmann, M. M. Carrasquillo, V. S. Pankratz, S. G Younkin, P. A. Holmans, M. O'Donovan, M. J. Owen, and J. Williams. Genome-wide association study identifies variants at clu and picalm associated with alzheimer's disease. *Nature Genetics*, 41(10):1088–1093, 2009.

[29] S. Calafate, W. Flavin, P. Verstreken, and D. Moechars. Loss of bin1 promotes the propagation of tau pathology. *Cell Reports*, 17(4):931–940, 2016.

[30] K. A. Boden, I. S. Barber, N. Clement, T. Patel, T. Guetta-Baranes, K. J. Brookes, S. Chappell, J. Craigon, N. H. Chapman, ARUK Consortium, K. Morgan, G. B. Seymour, and A. Bottley. Methylation profiling rin3 and mef2c identifies epigenetic marks associated with sporadic early onset alzheimer's disease. *Journal of Alzheimer's Disease Reports*, 1(1):97–108, 2017.

[31] Xiaohe Tian, Diana Leite, Edoardo Scarpa, Sophie Nyberg, Gavin Fullstone, Joe Forth, Diana Matias, Azzurra Apriceno, Alessandro Poma, Aroa Castano, Manish Vuyyuru, Lena Harker-Kirschneck, Andela Saric, Zhongping Zhang, Pan Xiang, Bin Fang, Yupeng Tian, Lei Luo, Loris Rizzello, and Giuseppe Battaglia. *On the shuttling across the blood-brain barrier via tubules formation: mechanism and cargo avidity bias*. 04 2020.

[32] A. Frost, R. Perera, A. Roux, K. Spasov, O. Destaing, E. H. Egelman, P. De Camilli, and V. M. Unger. Structural basis of membrane invagination by f-bar domains. *Cell*, 132(5):807–817, 2008.

[33] T. Itoh, K. S. Erdmann, A. Roux, B. Habermann, H. Werner, and P. De Camilli. Dynamin and the actin cytoskeleton cooperatively regulate plasma membrane invagination by bar and f-bar proteins. *Developmental Cell*, 9(6):791–804, 2005.

[34] J. Kostan, U. Salzer, A. Orlova, I. Toro, V. Hodnik, Y. Senju, J. Zou, C. Schreiner, J. Steiner, J. Merilainen, M. Nikki, I. Virtanen, O. Carugo, J. Rappsilber, P. Lappalainen, V.-P. Lehto, G. Anderluh, E. H. Egelman, and K. Djinovic-Carugo. Direct interaction of actin filaments with f-bar protein pacsin2. *EMBO Reports*, 15(11):1154–1162, 2014.

[35] B.-J. de Kreuk, M. Nethe, M. Fernandez-Borja, E. C. Anthony, P. J. Hensbergen, A. M. Deelder, M. Plomann, and P. L. Hordijk. The f-bar domain protein pacsin2 associates with rac1 and regulates cell spreading and migration. *Journal of Cell Science*, 124(Pt 14):2375–2388, 2011.

[36] T. Kanekiyo, H. Xu, and G. Bu. Apoe and aβin alzheimer's disease: accidental encounters or partners? *Neuron*, 81(4):740–754, 2014.

[37] V. Anggono, Y. Koç-Schmitz, J. Widagdo, J. Kormann, A. Quan, C.-M. Chen, P. J. Robinson, S.-Y. Choi, D. J. Linden, M. Plomann, and R. L. Huganir. Pick1 interacts with pacsin to regulate ampa receptor internalization and cerebellar long-term depression. *Proceedings of the National Academy of Sciences of the United States of America*, 110(34):13976–13981, 2013.

[38] H. Stenmark. Rab gtpases as coordinators of vesicle traffic. *Nature Reviews Molecular Cell Biology*, 10(8):513–525, 2009.

[39] J. L. Jankowsky, D. J. Fadale, G. M. Anderson, J.and Xu, V. Gonzales, N. A Jenkins, N. G. Copeland, M. K Lee, L. H. Younkin, S. L. Wagner, S. G. Younkin, and D. R. Borchelt. Mutant presenilins specifically elevate the levels of the 42 residue beta-amyloid peptide in vivo: evidence for augmentation of a 42-specific gamma secretase. *Human Molecular Genetics*, 13(2):159–170, 2004.

[40] I. Singh, A. P. Sagare, M. Coma, D. Perlmutter, R. Gelein, R. D. Bell, R. J. Deane, E. Zhong, M. Parisi, J. Ciszewski, R. T. Kasper, and R. Deane. Low levels of copper disrupt brain amyloid-β homeostasis by altering its production and clearance. *Proceedings of the National Academy of Sciences*, 2013.

[41] T. Kanekiyo, J. R. Cirrito, C.-C. Liu, M. Shinohara, J. Li, D. R. Schuler, M. Shinohara, D. M. Holtzman, and G. Bu. Neuronal clearance of amyloid-beta by endocytic receptor lrp1. *Journal of Neuroscience*, 33(49):19276–19283, 2013.

[42] S. Xu, M. Edman, M. S Kothawala, G. Sun, L. Chiang, A. Mircheff, L. Zhu, C. Okamoto, and S. Hamm-Alvarez. A rab11a-enriched subapical membrane compartment regulates a cytoskeleton-dependent transcytotic pathway in secretory epithelial cells of the lacrimal gland. *Journal of Cell Science*, 124(Pt 20):3503–3514, 2011.

[43] N. Yui, H. A. J. Lu, Y. Chen, N. Nomura, R. Bouley, and D. Brown. Basolateral targeting and microtubule-dependent transcytosis of the aquaporin-2 water channel. *American Journal of Physiology Cell Physiology*, 304(1):C38–48, 2013.

[44] A. M. Cataldo, C. M. Peterhoff, J. C. Troncoso, T. Gomez-Isla, B. T. Hyman, and R. A. Nixon. Endocytic pathway abnormalities precede amyloid beta deposition in sporadic alzheimer's disease and down syndrome: differential effects of apoe genotype and presenilin mutations. *The American Journal of Pathology*, 157(1):277–286, 2000.

[45] A. M. Cataldo, S. Petanceska, N. B. Terio, C. M. Peterhoff, R. Durham, M. Mercken, P. D. Mehta, J. Buxbaum, V. Haroutunian, and R. A. Nixon. Abeta localization in abnormal endosomes: association with earliest abeta elevations in ad and down syndrome. *Neurobiology of Aging*, 25(10):1263–1272, 2004.

[46] W. Xu, F. Fang, J. Ding, and C. Wu. Dysregulation of rab5-mediated endocytic pathways in alzheimer's disease. *Traffic*, 19(4):253–262, 2018.

[47] J. Chapuis, F. Hansmannel, M. Gistelinck, A. Mounier, C. Van Cauwenberghe, K. V. Kolen, F. Geller, Y. Sottejeau, D. Harold, P. Dourlen, B. Grenier-Boley, Y. Kamatani, B. Delepine, F. Demiautte, D. Zelenika, N. Zommer, M. Hamdane, C. Bellenguez, J.-F. Dartigues, J.-J. Hauw, F. Letronne, A.-M. Ayral, K. Sleegers, A. Schellens, L. V. Broeck, S. Engelborghs, P. P. De Deyn, R. Vandenberghe, M. O'Donovan,

M. Owen, J. Epelbaum, M. Mercken, E. Karran, M. Bantscheff, G. Drewes, G. Joberty, D. Campion, J.-N. Octave, C. Berr, M. Lathrop, P. Callaerts, D. Mann, J. Williams, L. Buee, I. Dewachter, C. Van Broeckhoven, P. Amouyel, D. Moechars, B. Dermaut, and J.-C. Lambert. Increased expression of bin1 mediates alzheimer genetic risk by modulating tau pathology. *Molecular Psychiatry*, 18(11):1225–1234, 2013.

[48] A. C. Pereira, J. D. Gray, J. F. Kogan, R. L. Davidson, T. G. Rubin, M. Okamoto, J. H. Morrison, and B. S. McEwen. Age and alzheimer's disease gene expression profiles reversed by the glutamate modulator riluzole. *Molecular Psychiatry*, 22(2):296–305, 2017.

[49] C.-H. Lin, E. Lin, and H.-Y. Lane. Genetic biomarkers on age-related cognitive decline. *Frontiers in Psychiatry*, 8:247, 2017.

[50] N. A. Stefanova, N. I. Ershov, K. Y. Maksimova, N. A. Muraleva, M. A. Tyumentsev, and N. G. Kolosova. The rat prefrontal-cortex transcriptome: Effects of aging and sporadic alzheimer's disease-like pathology. *The Journal of Gerontology A*, 74(1):33–43, 2019.

[51] L. Jones, P. A. Holmans, M. L. Hamshere, D. Harold, V. Moskvina, D. Ivanov, A. Pocklington, R. Abraham, P. Hollingworth, R. Sims, A. Gerrish, J. S. Pahwa, N. Jones, A. Stretton, A. R. Morgan, S. Lovestone, J. Powell, P. Proitsi, M. K. Lupton, C. Brayne, D. C. Rubinsztein, M. Gill, B. Lawlor, A. Lynch, K. Morgan, K. S. Brown, P. A. Passmore, D. Craig, B. McGuinness, S. Todd, C. Holmes, D. Mann, A. D. Smith, S. Love, P. G Kehoe, S. Mead, N. Fox, M. Rossor, J. Collinge, W. Maier, F. Jessen, B. Schürmann, R. Heun, H. Kölsch, H. van den Bussche, I. Heuser, O. Peters, J. Kornhuber, J. Wiltfang, M. Dichgans, L. Frölich, H. Hampel, M. Hüll, D. Rujescu, A. M. Goate, J. S. K. Kauwe, C. Cruchaga, P. Nowotny, J. C. Morris, K. Mayo, G. Livingston, N. J Bass, H. Gurling, A. McQuillin, R. Gwilliam, P. Deloukas, A. Al-Chalabi, C. E. Shaw, A. B. Singleton, R. Guerreiro, T. W. Mühleisen, M. M. Nöthen, S. Moebus, K.-H. Jöckel, N. Klopp, H.-E. Wichmann, E. Rüther, M. M. Carrasquillo, V. S. Pankratz, S. G. Younkin, J. Hardy, M. C. O'Donovan, M. J. Owen, and J. Williams. Genetic evidence implicates the immune system and cholesterol metabolism in the aetiology of alzheimer's disease. *PLoS One*, 5(11):e13950, 2010.

[52] M. Seifi, S. Rodaway, U. Rudolph, and J. D. Swinny. Gaba$_A$ receptor subtypes regulate stress-induced colon inflammation in mice. *Gastroenterology*, 155(3):852–864.e3, 2018.

Supporting Information

Cell culture. Human brain microvascular endothelial cells (HBMEC) were kindly provided by Prof Vivaldo Moura Neto (Universidade Federal do Rio de Janeiro, Brazil). HBMEC (between passage 6-15) were grown in Dulbecco's Modified Eagle Medium (DMEM) Glutamax supplemented with 10% (v/v) FBS and 100 IUL mL^{-1} penicillin/100 mg mL^{-1} streptomycin. Cells were maintained at 37 °C in an atmosphere of 5% CO2. For subculture, HBMEC cells were washed twice with PBS, incubated with 0.25% trypsin-EDTA for 3 minutes, centrifuged and resuspended in fresh media. Media was changed every 2-3 days.

Western blot. Polarised bEnd3 were washed twice with PBS and RIPA buffer containing protease inhibitors (1:50) was added directly to the membranes and left on ice for 1 hour. Cells were collected, centrifuged and the supernatant was collected for Western Blot analysis. Healthy (WT) mice were anesthetised, decapitated and the brains were carefully collected from the skull. Brains were homogenised in a 4-fold excess volume of ice-cold buffer solution: 10 mM HEPES, 141 mM NaCl, 4 mM KCl, 2.8 mM $CaCl_2$, 1 mM $MgSO_4$, 1 mM NaH_2PO_4 and 10 mM glucose, pH 7.4, in a glass homogeniser (10-15 strokes). Brain homogenates were resuspended in RIPA lysis buffer containing protease inhibitors (1:50), centrifuged for 20 minutes, and the supernatant used for Western blot analysis. Protein levels in the lysates were determined using BCA Protein Assay Kit. Lysates were mixed with Laemmli sample buffer and proteins (10 μg) were separated on 10% SDS polyacrylamide gels and transferred to polyvinylidene difluoride (PVDF) membranes. Membranes were blocked with 5% (w/v) non-fat milk in Tris-buffered saline (TBS) containing 0.1% (w/v) Tween-20 (TBS-T) for 1 hour and then incubated with a rabbit monoclonal antibody to LRP1 overnight at 4 °C. After washing with TBS-T, the membranes were incubated with a secondary antibody for 2 hours at room temperature and imaged using an Odyssey CLx (LI-COR Biosciences). The membranes were further probed for GAPDH as a loading control.

Immunofluorescence. Polarised bEnd3 monolayers were fixed in 4% (w/v) PFA for 15 minutes, permeabilised with 0.1% (w/v) Triton X-100 in PBS for 10 minutes and incubated with 5% (w/v) BSA in PBS for 1 hour at room temperature. Then, cell monolayers were incubated with primary antibodies diluted in 1% (w/v) BSA and 0.01% (w/v) Triton X-100 in PBS overnight at 4 ºC, followed by washing with PBS and incubation with the corresponding secondary antibodies for 2 hours at room temperature. Nuclei was stained by incubation with DAPI for 10 minutes. Transwell membranes were excised using a scalpel and mounted on co-verslips with Vectashield Mounting Media. Colocalisation analysis was carried out using coloc2 plugin in Image J. Coronal brain sections were obtained from adult healthy (WT) and AD (TG) mice. Briefly, brain sections were incubated in 20% (v/v) normal horse serum in PBS containing 0.3% (w/v) Triton X-100 for 2 hours at room temperature under gentle agitation followed by incubation with primary antibodies overnight at 4 °C. Sections were washed with PBS, incubated with the corresponding secondary antibody and FITC-conjugated lectin (1:200) for 2 hours and washed with PBS. Brain sections were mounted on glass slides in Vectashield Mounting Media.

Table 1 List of antibodies.

Antibody	Dilution	Supplier, Catalogue Number
Rabbit polyclonal to syndapin-2 †	1:400	Abcam, ab37615
Mouse monoclonal to LRP1	1:100	Sigma, L2420
Mouse monoclonal to LRP1 ⋆	1:1000	Invitrogen, 37-7600
Rabbit monoclonal to LRP1 †	1:1000	Abcam, ab92544
Mouse monoclonal to GAPDH †	1:1000	Abcam, ab8245
Mouse monoclonal to ApoE	1:200	Novus Biologicals, NB110-60531
Mouse monoclonal to EEA-1	1:100	Sigma, E7659
Rabbit polyclonal to EEA-1	1:100	Abcam, ab2900
Mouse monoclonal to Rab5 †	1:400	Sigma, R7904
Rabbit polyclonal to Rab5	1:100	Abcam, ab13253
Mouse monoclonal to Rab7	1:100	Sigma, R8879
Rabbit polyclonal to Rab7	1:100	Abcam, ab137029
Mouse monoclonal to Aβ	1:1000	Biolegend, 800708
Alexa Fluor 488 goat anti-mouse IgG	1:500	Biolegend, 405319
Alexa Fluor 647 donkey anti-rabbit IgG	1:500	Biolegend, 406414
Dylight 800 goat anti-mouse IgG †	1:5000	Thermo Fisher Scientific, SA535521
Dylight 800 goat anti-rabbit IgG †	1:5000	Thermo Fisher Scientific, SA535571

† Antibodies used for western blot. ⋆ Antibodies used in immunohistochemistry.

***In Vitro* Permeability of Aβ (1-40).** To evaluate the permeability of Aβ across the polarised bEnd3 monolayers, FAM-Aβ(1-40) (500 nM) was added to the apical side of the transwell to measure apical-to-basal permeability. Samples were collected from the basal side, and fresh medium was added to replace the volume. FAM-Aβ(1-40) fluorescence was measured in a 96-well plate using a Spark Multimode microplate reader (Tecan). Apparent permeability was calculated as:

$$P = \frac{V_r}{C_0 A} \frac{dQ}{dt} \tag{2}$$

with V_r being the volume of the receptor (basal), C_0 the initial Aβ concentration, A the total surface area of the transwell membrane, and $\frac{dQ}{dt}$ the transport rate calculated as the gradient of mass over time.

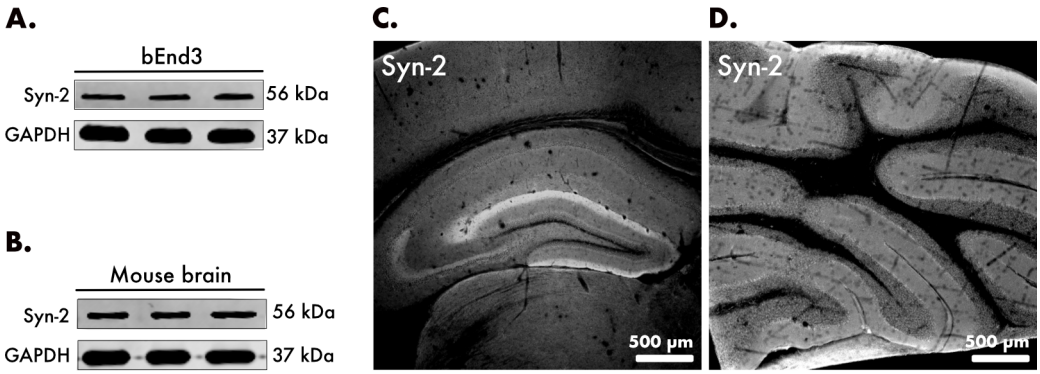

Figure S1: Expression of syndapin-2 in the brain endothelium and mouse brain. Immunoblotting for syndapin-2 and GAPDH (loading) control in (**A**) polarised BECs (bEnd3) and (**B**) WT mouse brains. n = 3. Immunocolocalisation of syndapin-2 in (**C**) hippocampus and (**D**) cerebellum in mouse brain.

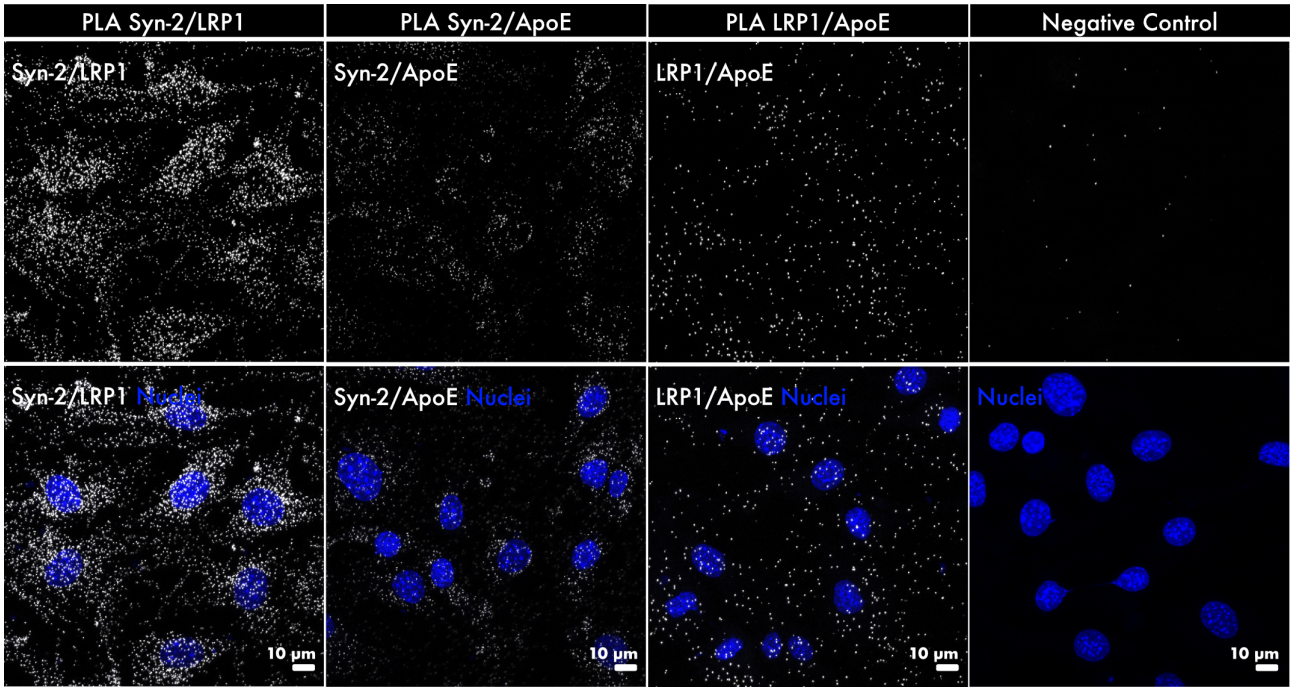

Figure S2: Association of syndapin-2 with LRP1 and ApoE in mouse BECs. Confocal images showing the abundance of PLA dots (white) resulting from the proximity of syndapin-2/LRP1, syndapin-2/ApoE and LRP1/ApoE within BECs. Nuclei are shown in blue. Image from the negative control confirmed the specificity of the PLA probes.

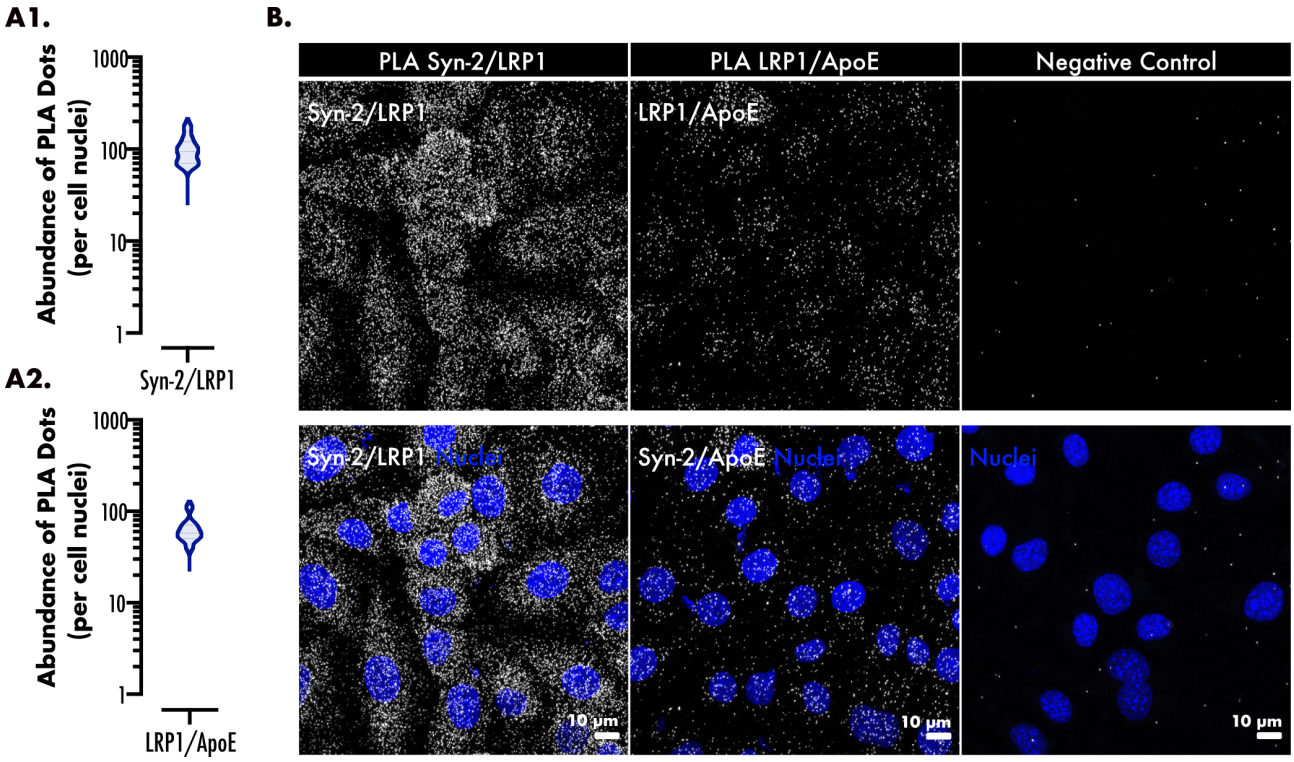

Figure S3: Association of syndapin-2 and LRP1 in human BECs. Abundance of PLA dots representing the proximity of (**A1**) of syndapin-2/LRP1 and (**A2**) LRP1/ApoE in human BECs. Violin plot of n = 10 cells. (**B**) Representative confocal images of the abundance of PLA dots (white) resulting from the proximity of syndapin-2/LRP1 and LRP1/ApoE. Nuclei are depicted in blue. Negative control confirmed the specificity of the PLA probes.

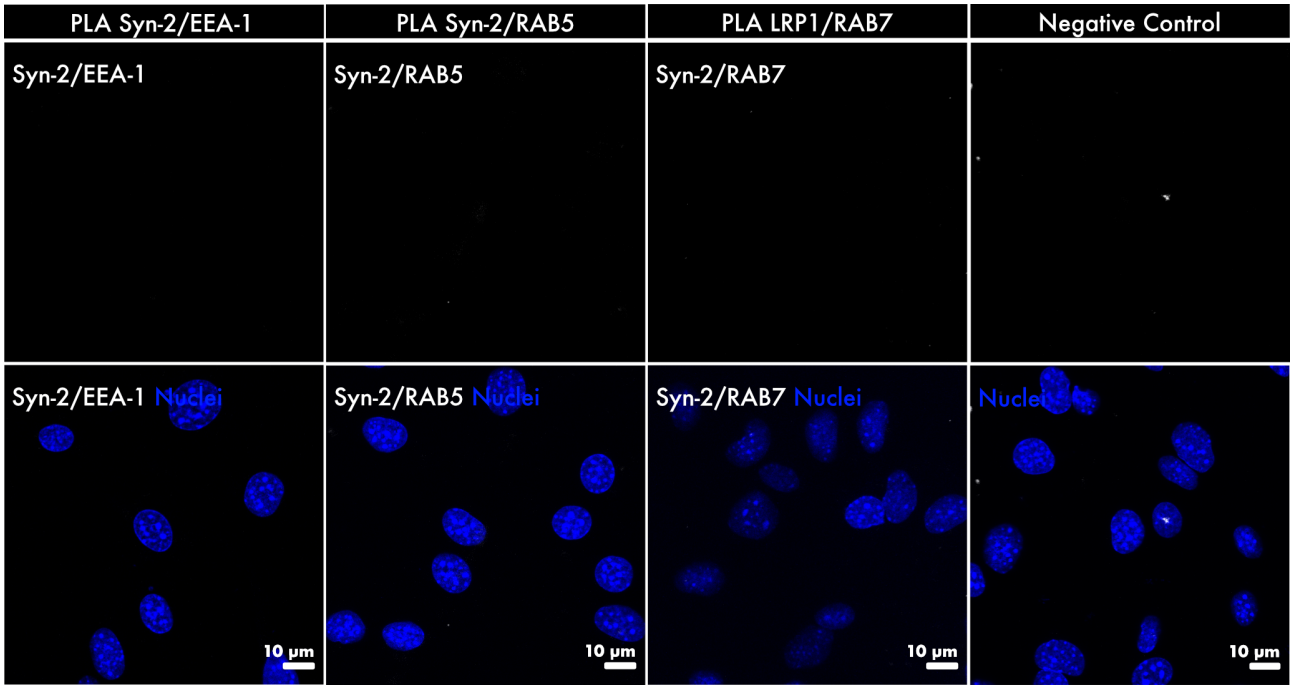

Figure S4: Syndapin-2 is not associated with vesicular endocytic proteins in BECs. Confocal images of the abundance of PLA dots (white) for syndapin-2/EEA-1, Rab5 and Rab7 in polarised mouse BECs. Nuclei are shown in blue. Negative control confirmed the specificity of the probes.

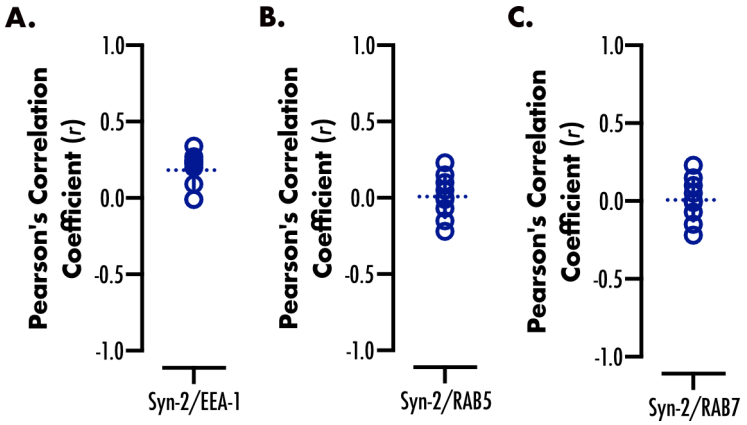

Figure S5: Colocalisation of syndapin-2 and vesicular endocytic proteins in BECs. Pearson's correlation coefficient of (**A**) syndapin-2/EEA-1, (**B**) syndapin-2/Rab5 and (**C**) syndapin-2/Rab7 in polarised BECs. Data are presented as mean $\pm$ SD (n = 10 images).

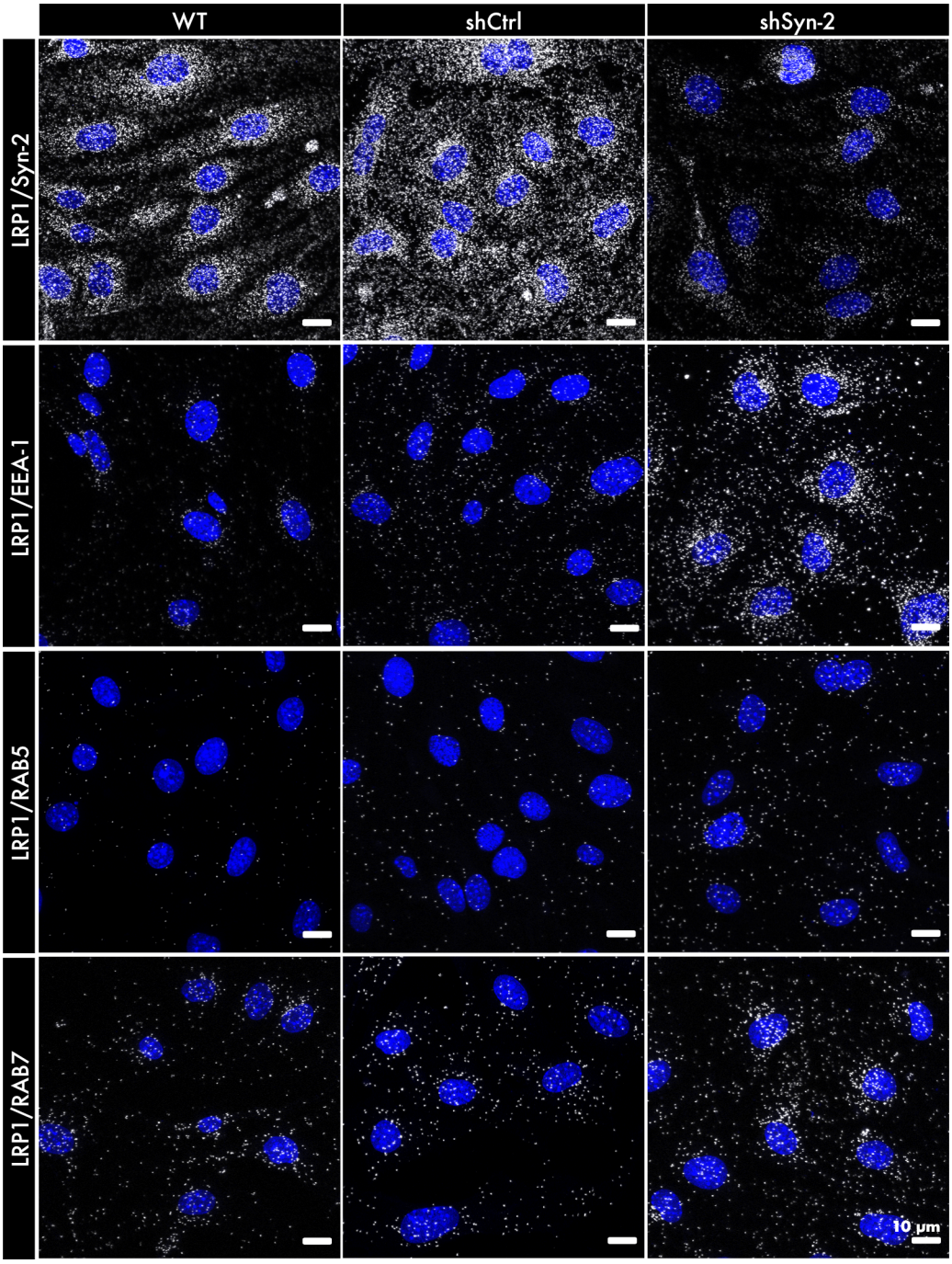

Figure S6: Balance between syndapin-2- and Rab-mediated LRP1 trafficking within BECs. Confocal images representing the abundance of PLA dots (white) for LRP1/syndapin-2, LRP1/EEA-1, LRP1/Rab5 and LRP1/Rab7 in wild-type (WT), shRNA control (shCtrl) and syndapin-2 knockdown (shSyn-2) BECs.

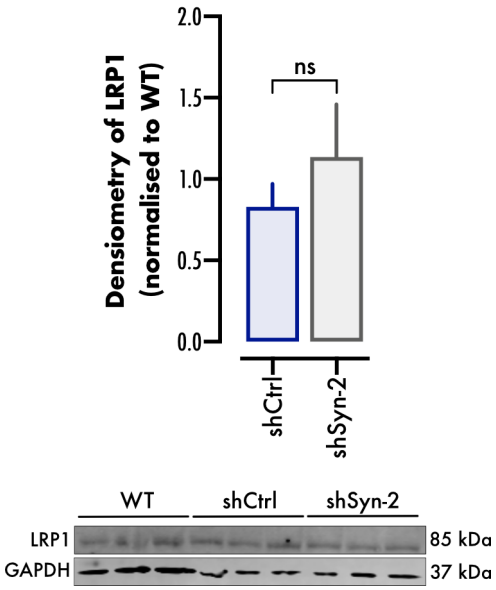

Figure S7: Expression of syndapin-2 in syndapin-2 knockdown BECs. Immunoblotting for LRP1 and GAPDH (loading control) in wild-type (WT), shRNA control (shCtrl) and syndapin-2 knockdown (shSyn-2) BECs. Relative abundance of LRP1 in BECs determined by densiometry analysis relative to GAPDH. Data are presented as mean $\pm$ SD (n = 3). NS, not significant.

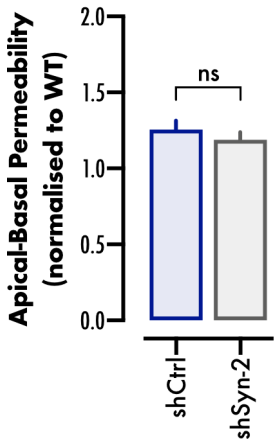

Figure S8: *In vitro* permeability of FAM-Aβ (1-40) across polarised BECs in the apical-to-basal direction (blood-to-brain). Permeability of FAM-Aβ (1-40) across polarised BECs expressing endogeneous (shCtrl) and lower levels of syndapin-2 (shSyn-2) in the basal-to-apical (brain-to-blood) direction. Permeability values were normalised to wild-type (WT) BECs. Mean $\pm$ SD (n = 15). NS, not significant.

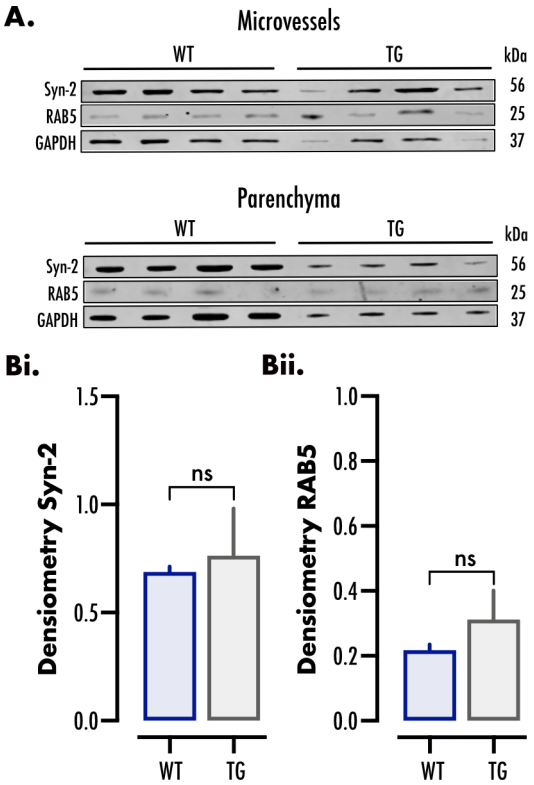

Figure S9: Alterations in expression of syndapin-2 and Rab5 in healthy and AD 4-months old mouse brains. (**A**) Immunoblotting for syndapin-2, Rab5 and GAPDH (loading control) in isolated microvessels from 4-months old WT and APP-PS1 mice. Relative abundance of (**Bi**) syndapin-2 and (**Bii**) Rab5 in microvessels from WT and APP-PS1 brains determined by densiometry analysis relative to GAPDH. Mean $\pm$ SD (n = 4 animals). NS, not significant.